STUDY OF CU(II):GLYCINE SOLUTION BY X-RAY

ABSORPTION SPECTROSCOPY

Kanchanasuda Klaiphet

A Thesis Submitted in Partial Fulfillment of the Requirements for the

Degree of Master of Science in Physics

Suranaree University of Technology

Academic Year 2019

การศึกษาสารละลายคอปเปอร์:ไกลซีนโดยใช้เทคนิคการดูดกลืนรังสีเอ็กซ์

นางสาวกาญจนสุดา กลายเพศ

วิทยานิพนธ์นี้เป็นส่วนหนึ่งของการศึกษาตามหลักสูตรปริญญาวิทยาศาสตรมหาบัณฑิต
สาขาวิชาฟิสิกส์
มหาวิทยาลัยเทคโนโลยีสุรนารี
ปีการศึกษา 2562

STUDY OF CU(II):GLYCINE SOLUTION BY X-RAY

ABSORPTION SPECTROSCOPY

Suranaree University of Technology has approved this thesis submitted in partial fulfillment of the requirement for a Master's Degree.
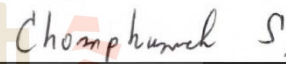
Thesis Examining Committee

_____

(Assoc. Prof. Dr. Puangratana Pairor)

Chairperson

_____

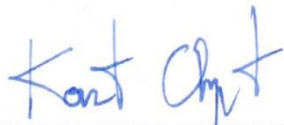(Assoc. Prof. Dr. Prayoon Songsiriritthigul)

Member (Thesis Advisor)

_____

(Dr. Chomphunuch Songsiriritthigul)

Member

_____

(Dr. Chatree Saiyasombat)

Member

_____   _____

(Assoc. Prof. Flt. Lt. Dr. Kontorn Chamniprasart) (Assoc. Prof. Dr. Worawat Meevasana)

Vice Rector for Academic Affairs   Dean of Institute of Science

and Internationalization

กาญจนสุดา กลายเพศ : การศึกษาสารละลายของคอปเปอร์:ไกลซีนโดยใช้เทคนิคการ
ดูดกลืนรังสีเอ็กซ์ (STUDY OF CU(II):GLYCINE SOLUTION BY X-RAY
ABSORPTION SPECTROSCOPY) อาจารย์ที่ปรึกษา : รองศาสตราจารย์ ดร.ประยูร
ส่งสิริฤทธิกุล, 72 หน้า.

วิทยานิพนธ์ฉบับนี้มุ่งเน้นการตรวจสอบโครงสร้างของสารละลายคอปเปอร์ไดคลอไรด์
(CuCl$_2$) ที่ทำปฏิกิริยารวมกับสารละลายไกลซีนด้วยเทคนิคการดูดกลืนรังสีเอ็กซ์ เทคนิคสเปกโทร
สโกปีการดูดกลืนรังสีเอ็กซ์ใกล้ขอบเขตการดูดกลืนรังสีเอ็กซ์ (X-ray absorption near edge
structure: XANES) สามารถใช้อธิบายผลของการเปลี่ยนแปลงโครงสร้างของสารละลายคอปเปอร์ :
ไกลซีนได้ โดยในอัตราส่วนของสารละลายจะมีค่าความเป็นกรด-เบสที่แตกต่างกัน ซึ่งเป็นตัวแปร
สำคัญที่มีอิทธิพลต่อการเปลี่ยนแปลงรูปแบบโครงสร้างของคอปเปอร์ และพบว่าที่ค่าความเป็น
กรด-เบสเท่ากับ 5 ไม่มีการเปลี่ยนแปลงโครงสร้างของสารละลายคอปเปอร์:ไกลซีน

เทคนิคสเปกโทรสโกปีการดูดกลืนรังสีเอ็กซ์สามารถวิเคราะห์การสร้างพันธะของอะตอม
คอปเปอร์กับอะตอมรอบข้างที่จะเข้ามาทำปฏิกิริยาโดยอะตอมเหล่านั้นมาจากไกลซีนและน้ำ ซึ่ง
สเปกตรัมของช่วงพลังงานที่จะศึกษานี้อยู่เหนือขอบการดูดกลืนรังสีเอ็กซ์ของอะตอมคอปเปอร์
หรือที่เรียกว่า EXAFS: Extended X-ray Absorption Fine Structure จากผลของการศึกษาสามารถ
ยืนยันได้ว่าอะตอมของคอปเปอร์จะสร้างพันธะกับอะตอมออกซิเจนหรือไนโตรเจนของสารละลาย
ไกลซีนที่ระยะ 1.9 อังสตรอม

สาขาวิชาฟิสิกส์	ลายมือชื่อนักศึกษา_____กาญจนสุดา กลายเพศ_____
ปีการศึกษา 2562	ลายมือชื่ออาจารย์ที่ปรึกษา_____

KANCHANASUDA KLAIPHET : STUDY OF CU(II):GLYCINE

SOLUTION BY X-RAY ABSORPTION SPECTROSCOPY. THESIS

ADVISOR : ASSOC. PROF. PRAYOON SONGSIRIRITTHIKUL, Ph.D.

72 PP.

SYNCHROTRON RADIATION/ X-RAY ABSORPTION SPECTROSCOPY/

XANES/ EXAFS

This experimental work focuses on the investigation of copper(II) chloride solutions mixed with glycine by using X-ray absorption spectroscopy technique. Structural changes of the mixture solutions are determined from X-ray absorption near-edge structure (XANES) spectra for various Cu(II):Glycine molar ratios. Interestingly, pH value is an important parameter since it influences the formation of the different copper species. There is no change of Cu(II):Glycine solution at pH 5.

The information on the coordination shells of the metallic center for various ratio of Cu(II):Glycine can be extracted from extended X-ray absorption fine structure (EXAFS) spectra. The investigation proposes the coordination distance of 1.9 Å for Cu(II):Glycine complex. This could be interesting point for the understanding of the interactions of metal ions with biomolecules as a basic knowledge for future applications.

School of Physics

Academic Year 2019

Student's Signature _Kanchanasuda Klaiphet_

Advisor's Signature _Prayoon Song._

ACKNOWLEDGEMENTS

Kanchanasuda Klaiphet

CONTENTS

CONTENTS (Continued)

LIST OF TABLES

LIST OF FIGURES

LIST OF FIGURES (Continued)

LIST OF FIGURES (Continued)

LIST OF FIGURES (Continued)

LIST OF FIGURES (Continued)

LIST OF FIGURES (Continued)

LIST OF ABBREVIATIONS

Å	Angstrom
°C	Degree Celsius
E	Energy
FT	Fourier Transform
RF	Radio Frequency
XAS	X-ray Absorption Spectroscopy
SYN	Synchrotron
STR	Storage ring
LBT	Low Energy Beam Transport line
HBT	High Energy Beam Transport line
DCM	Double Crystal Monochromator
SLRI	Synchrotron Light Research Institute
XAFS	X-ray Absorption Fine Structure
LMCT	Ligand to Metal Charge Transfer
XANES	X-ray Absorption Near Edge Structure
EXAFS	Extended X-ray Absorption Fine Structure
BL1.1W	Beamline 1.1W
LINAC	Linear Accelerator

CHAPTER I

INTRODUCTION

Metal ions play an important role in various functions of biological processes. In living organisms, most metal ions interact with proteins and can activate enzymatic properties. In human body, copper is the third most abundant transition-metal, following iron and zinc and mainly exists in the divalent oxidation number (Carrera *et al*., 2004). Copper can be found in many types of food, drinking water and in air. Human absorbs copper into body everyday by eating, drinking and breathing. Copper is a common substance found in the environment and spreads through natural phenomena. Humans widely use copper. For instance, it is used in the industry and agriculture. For this reason, the amount of copper in the environment increases. Copper production is still increasing, this means more copper in the environment. Rivers are a large reservoir of sludge contaminated with copper from a removal of wastewater containing copper. Copper in air, most are released during fuel combustion. Copper also can be released from human activities such as mining, metal production, wood production, and phosphate fertilizer production. Copper absorption is necessary because copper is essential for human health. Although human can handle the concentration of copper in large quantities, too much copper can cause health problems.

The building blocks of proteins are called amino acids. Any free amino acid and any protein exist in the form of a zwitterions (zwitterion: an equal number of positively and negatively charged groups). The simplest amino acid is a glycine, which is the first

amino acid this covered. Glycine can be existed both as an acid (protonated form) and base (deprotonated form) in aqueous solution. In the living organism, interaction between copper ions and glycine is important for breathing process. Generally, the knowledge of metal ions interact with amino acid which is important for a better understanding of various chemical processes occurring in living organisms.

To understand the function of copper in living organisms, it is important to understand how copper atoms are bonded to amino acid. In this work, a simple amino acid such as glycine was chosen for the study. X-ray absorption near-edge structure (XANES) spectra of copper K-edge will be measured. The mixture solutions of Cu(II):Glycine at high and low concentration at different pH and also adjustment pH was examined. Structural changes in the mixture solutions was deduced from the spectra. The coordination shell of neighboring atoms were extracted from extended X-ray absorption fine structure (EXAFS) spectra.

In this work, we focused on structural change of Cu(II):Glycine with varying molar ratios by X-ray absorption near-edge structure (XANES) technique and study coordination shells of the metallic center by extended X-ray absorption fine structure. Structural behavior change of glycine species was observed when a different pH value and varied concentration. At low concentration of copper(II) chloride and glycine complex solutions were focused. Furthermore, experimental limits were defined by X-ray absorption spectroscopy technique at beamline 1.1W: multiple X-ray techniques of SLRI, Thailand. Cu(II): Glycine aqueous solutions studied at high (0.5 M and 0.25M) and low (1.5 mM) concentration. The molar ratio for the solutions used will be compiled with the instrumentation sensitivity.

CHAPTER II

THEORY / LITERATURE REVIEW

2.1 Copper Metal

2.1.1 Properties of copper in human

It has long been known that transition metals such as iron, cobalt, copper, zinc, and manganese play an important role in biological processes, whereas lead, cadmium, and mercury are toxic for many living systems. Copper exists in human body, mostly with the number of oxidation of 2+. It is the third most abundant in human body after iron and zinc, respectively (Carrera *et al*., 2004). Interestingly, Copper is an essential trace element vital to the health of all living organisms. In human body, copper is found around 2 mg per weight of body (*EFSA*, 2015). Copper is found throughout the body, it is concentrated in organs with high metabolism, such as the liver, kidney, hearth and brain. The tiny amount is enough to provide copper ions for billions of protein molecules, in particular enzymes.

Practically every cell in the body utilizes copper and together with iron and zinc, copper is one of the essential minerals to best health. Copper is vital to the health of the body from fetus development through to old age, as shown in Table 2.1. Without copper our brains, nervous systems and cardiovascular system could not function normally.

Table 2.1 Summary of adequate intake for copper (*EFSA*, 2015)

Age	adequate copper intakes (mg/day)	
	Female	**Male**
7 − 11 months	0.4	0.4
1 − <3 years	0.7	0.7
3 − <10 years	1.0	1.0
10 − <18 years	1.1	1.3
≤18 years	1.3	1.6
Pregnancy	1.5	
Lactation	1.5	

2.1.2 Properties of copper solution

Transition metals have more than one common oxidation state: copper compounds have forms with oxidation state 1+ (cuprous) and 2+ (cupric). Normally, copper at ground state has the configuration which is $4s^2 3d^9$, if 4s orbital lose one electron to 3d orbital that has the configuration $4s^1 3d^{10}$. The oxidation state of copper is stabilized in the solid phase with oxidation state 1+. Otherwise, the oxidation state of copper in liquid phase is Cu^{2+} due to copper dominates ions in aqueous chemistry (Moira, 2013).

The Pourbaix diagram shows the thermodynamically stable form of an element as a function of standard reduction potential and pH (Moira, 2013). The pH and standard electrod potential (E^0) are used to map the boundaries between the various oxidation states; the stable states are shown at the different pH values. For ammonium copper aqueous system which depends on the electrons (potential) and pH of the

solution, either Cu(I) and Cu(II) amine species can exist in solution. Figure 2.1 showed potential (E_H)-pH diagram for Cu-H_2O-NH_3, the Cu(I) species ($Cu(NH_3)_2^+$ is stable at about 5 to 12 of pH and E_H about -0.2 to 0.2 V. The Cu(II) species ($Cu(NH_3)_4^{2+}$ is stable about 8.5 to 11.5 of pH and E_H about -0.15 to 1.3 V (Konishi, 2007).
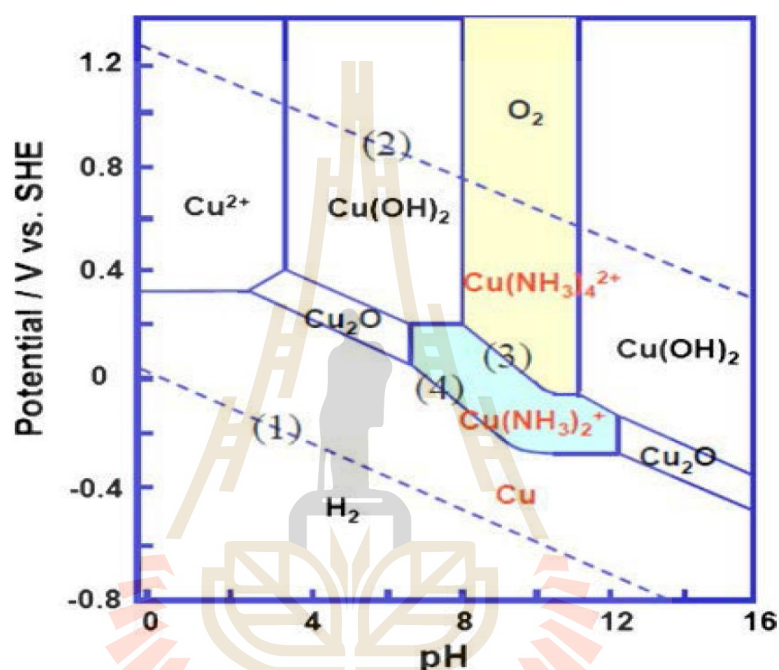
Figure 2.1 Potential-pH diagram of Cu-H_2O-NH_3 system at 25°C (Konishi, 2007).

Figure 2.2 showed the Pourbaix diagram containing the three different types of lines that show the equilibrium conditions for the given element (Mairo, 2013). Horizontal lines indicate pure redox transformations and the boundaries depend on potential. Vertical lines indicate an equilibrium that depend on pH. The diagram lines represent redox potentials of a solution in equilibrium which involves hydroxide or hydrogen ions.
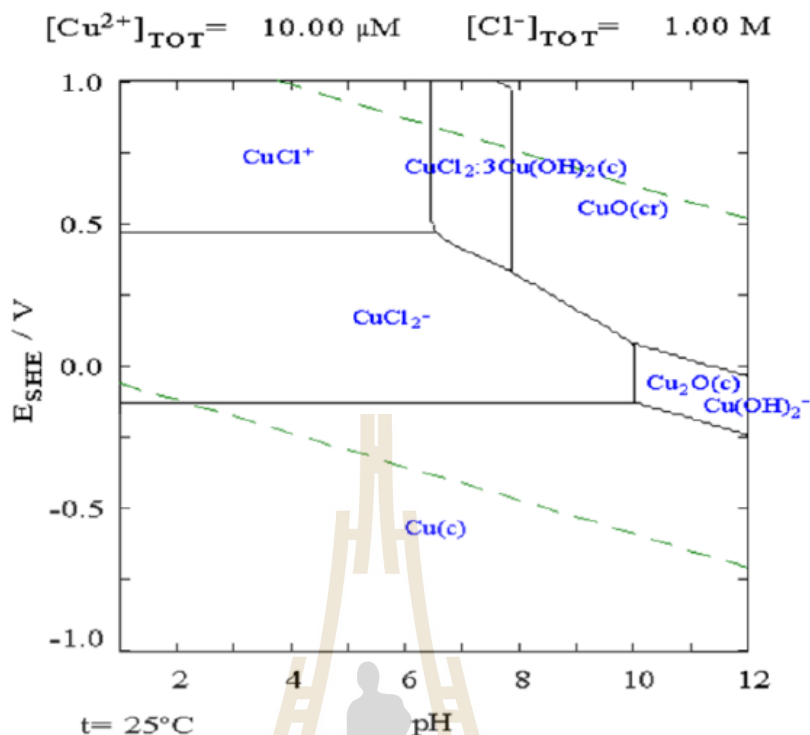
Figure 2.2 Potential-pH diagram of Copper(II) chloride solution (Moira, 2013).

2.2 Properties of Glycine

Proteins are linear polymers formed by linking peptide bonds of amino acids. Amino acids are a group of organic molecules that consist of a basic amino group (NH_2), an acidic carboxyl group (COOH) and the R group (or side chain) as shown in Figure 2.3. A central carbon (C) atom or α-carbon is a component of each molecule, in both an amino and carboxyl groups are attached. The remaining two bonds of the α-carbon atom are generally with a hydrogen (H) and the R group. Molecules of amino acids are composed of two parts, i.e. "backbone" and "side chain". Backbone is the similar part of each molecule (building block), and the side chain is a part for determining the type of amino acid (different side chain, different name of amino acid).

Amino acids have a common chemical formula: NH_2-CHR-COOH (Sompornpisut, 2009).
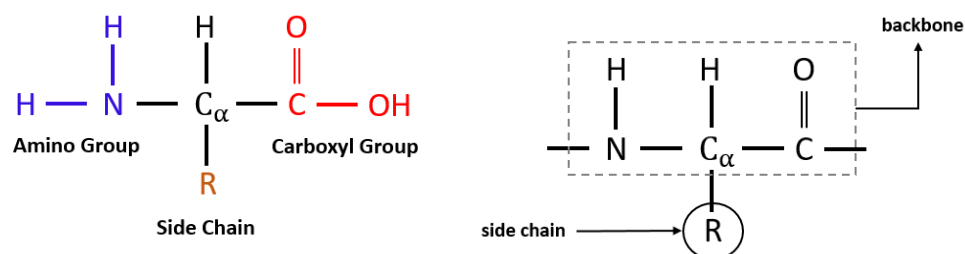
Figure 2.3 Typical structure of amino acid (Sompornpisut, 2009).

Glycine (NH_2CH_2COOH), is the simplest and smallest possible amino acid among 20 types that are found in nature. Moreover, the human body can synthesize glycine. In aqueous solution, zwitterion of glycine solution can express in both an acid and a base. pH also affects to the moleclue of zwitterion, at low pH the molecule can be protonated with a pK_a at about 2.35 and at high pH it loses of proton with pK_a at about 9.78, as shows in equations 2.1 and 2.2.

$$+H_3NCH_2COOH_{(aq)} \leftrightarrows +H_3NCH_2COO^-_{(aq)} + H^+_{(aq)} \quad pK_{a1} = 2.35 \quad (2.1)$$

$$+H_3NCH_2COO^-_{(aq)} \rightleftarrows H_2NCH_2COO^-_{(aq)} + H^+_{(aq)} \quad pK_{a2} = 9.78 \quad (2.2)$$
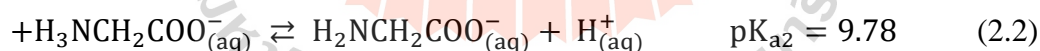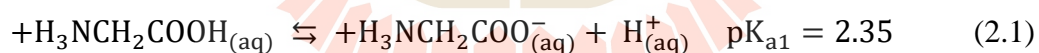
The different pH value can identifying the formation of glycine solution by titration curve glycine solution, shown in Figure 2.4.
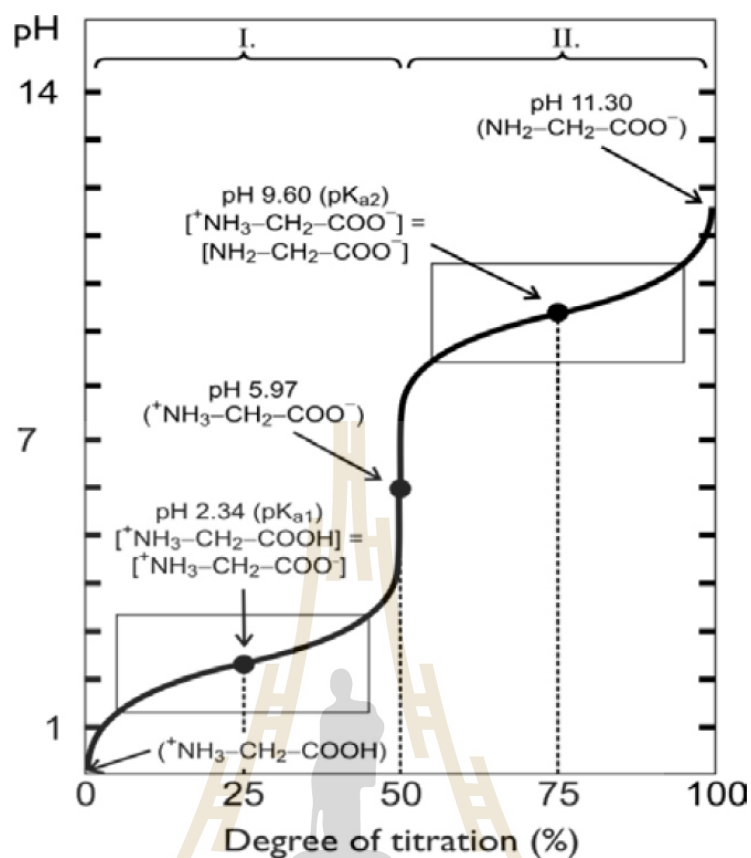
Figure 2.4 Titration curve of glycine solution with NaOH (Tanda, 2017).

2.3 Behavior of Copper and Glycine

Interactions between metal ions and proteins occur in living organisms. Naturally, amino acids which form the proteins may form stable five-membered chelate rings with metal ions, where the donor groups are amino N_{am} and carboxylate O_{COO} groups (Carrera *et al.*, 2004). Interaction between metal ions and amino acids are common both in solution and gas phase (Remko *et al.*, 2006). Such finding was concluded from the results of the computational studies on the effect of metal ions and water on the relative stability and geometric structure of non-zwitterionic and zwitterionic species of glycine by using B3LYP hybrid functional. Structures of

Gly·M^{n+}(H_2O)$_m$ and GlyZwitt·M^{n+}(H_2O)$_m$ (M^{n+} =L$^+$, Na$^+$, K$^+$, Mg^{2+}, Ca^{2+}, Ni^{2+}, Cu^{2+} and Zn^{2+} ; $m = 0, 2\ 5$) complexes were investigated. It was found that the suitable initial geometries of glycine complexes with monovalent and divalent cations are from dicoordinated complexes of glycine as shows in Figure 2.5. At m = 0, amino acids formed stable five-membered chelate rings with metal cations.
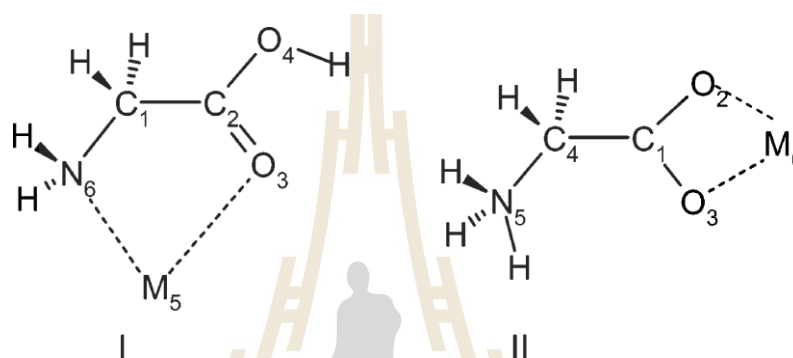
Figure 2.5 The structure of chelated glycine (I) and the zwitterionic form of glycine (II) (Remko *et al.*, 2006).

In 1998, D'Angelo *et al*. reported structure of bis(glycinato)copper(II) complex in aqueous solution investigated by X-ray absorption spectroscopic technique. The findings help understanding of the binding of the ions in biological compounds of cupric ions with amino acids. The structure of bis(glycinato)copper(II) has a distorted octahedral geometry with two glycine ligands coordinating to the Cu^{2+} ion in the equatorial plane and with the axial sites occupied by two additional water molecules at 2.40 ± 0.06 Å. Figure 2.6 showed the geometry of the structure of bis(glycine)copper(II) complex in aqueous solution. The structural parameters as derived from EXAFS data analysis are given in table 2.2. The best-fit analysis of the EXAFS spectrum is in the

range $k = 2.5\text{-}14.6$ Å^{-1}. The first two peaks in the FT at ~1.6 and 2.4 Å^{-1} are Cu-glycine

and Cu-O$_{ax}$ signals, as shown in Figure 2.7.
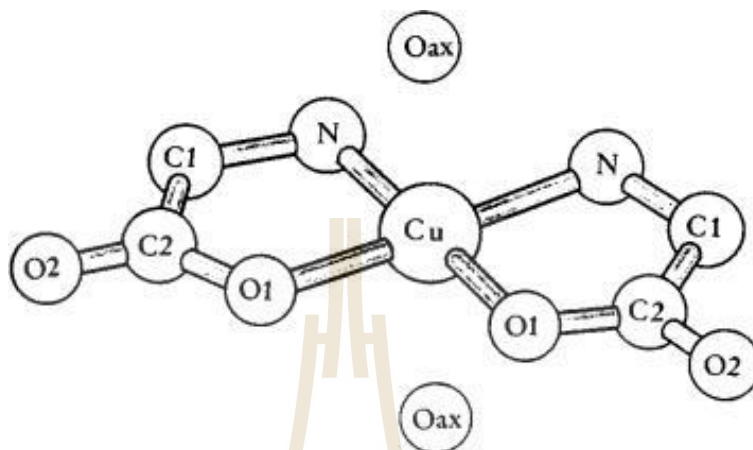
Figure 2.6 Geometry of the *cis*-bis(glycinato)copper(II) dehydrate complex in aqueous

solution (Angelo *et al.*, 1998).
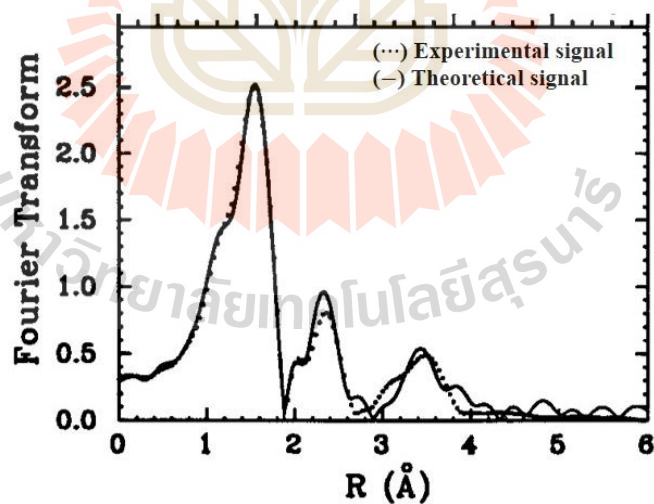
Figure 2.7 Comparison of the theoretical (solid line) and experimental (dotted line)

signals of the *k*-weighted EXAFS data and FT of bis(glycinato)copper(II)

complex (Angelo *et al.*, 1998).

Table 2.2 The parameters of *cis*-bis(glycinato)copper(II) monohydrate(Angelo *et al.*, 1998).

Structural feature	CN	Distance (Å)	σ^2 (Å^2)
Cu-O$_1$	2	1.95	0.004
Cu-N	2	1.99	0.004
Cu-O$_{ax}$	2	2.4	0.03
Cu-O$_s$	4	3.3	0.06

The bis(glycinato)copper(II) complex in an aqueous solution contains one molecule of copper and two molecules of glycine. In their work, the structure of such complex was investigated.

In 1996, Darj and co-workers studied the concentration profiles and the visible spectra of copper species. They used the window factor analysis (WFA) method to extract the concentration profiles of the complexes between Cu(II) and glycine in the acid region. The visible absorption spectra were recorded for aqueous acid solutions with various concentrations. The solutions contain 0.002 M Cu(II) and 0.500 M glycine with pH ranging from 1.0 to 7.0. Twenty-two solutions of copper-glycine were examined. Four copper species, i.e. Cu^{2+}, $CuGlyH^{2+}$, $CuGly^+$ and $CuGly_2$ were found. The concentration profiles as a function of pH is shown in Figure 2.8. At the pH value of more than 5, only one copper species, i.e. $CuGly_2$, exists.
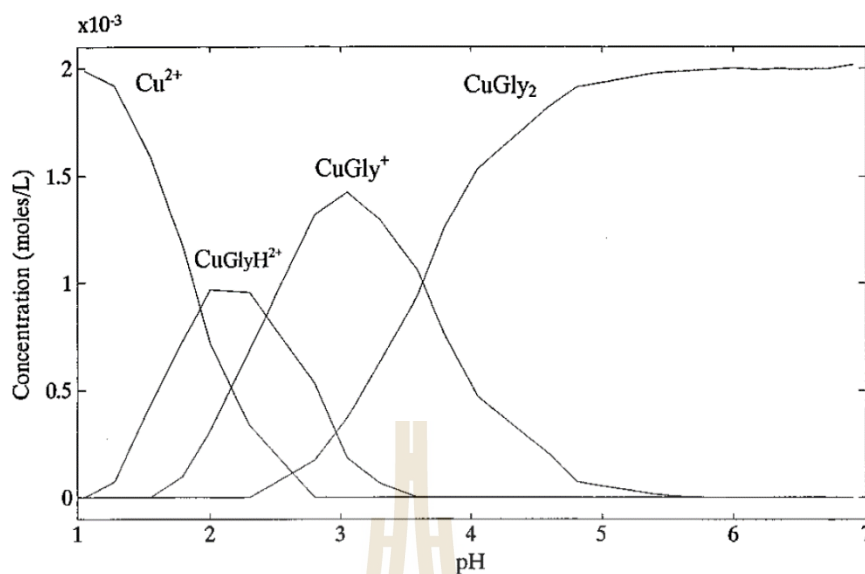
Figure 2.8 The concentration profiles of four copper species i.e. Cu^{2+}, $CuGlyH^{2+}$, $CuGly^+$, and $CuGly_2$ (Darj *et al.*, 1996).

Carrera *et al.* investigated the structural of $CuGly_2$ by X-ray absorption spectroscopy in 2004. They focused on the metal-ligand coordination distances in the solution of Cu(II) cations and amino acid glycine for 1:2 metal to amino acid ratio at pH of 7.3 and at low concentrations. They compared results between theory and experiment for the coordination distance of $CuGly_2$. The EXAFS spectra analysis was carried out for the first shell, which consists of two nitrogen atoms and two oxygen atoms, as shown in Figure 2.9. The average value of the Cu-N coordination distance is 2.00 Å and that of Cu-O is 1.955 Å.
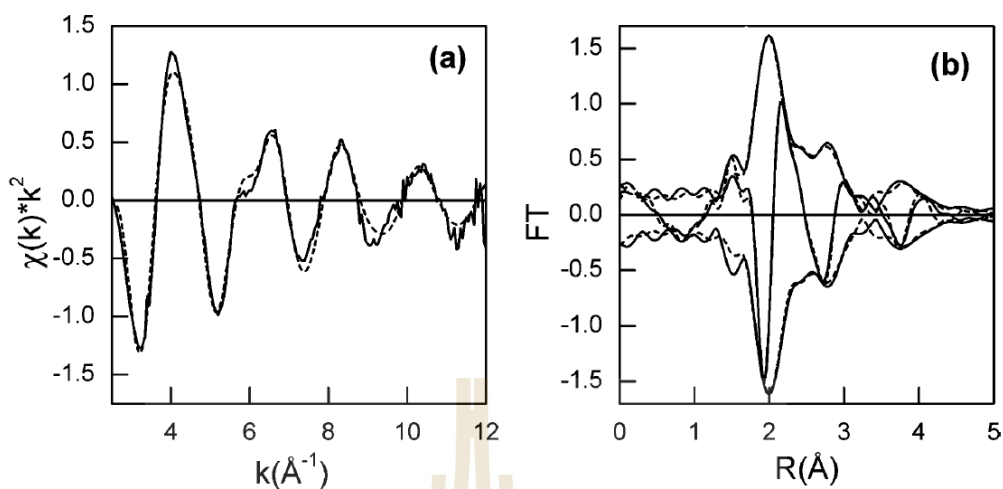
Figure 2.9 (a) Raw EXAFS data, k^2-weighted, of CuGly2: Experimental function (solid

line) and spectrum obtained by using the parameters included in table 2.3

(dashed line) (b) Cu-N phase corrected Fourier transform of the EXAFS

spectra included in Figure 2.9(a) magnitude and imaginary part:

experimental (solid line); best fit (dashed line) (Carrera *et al.*, 2004).

Table 2.3 Structural parameters of Cu(Gly)2 obtained from the EXAFS Fit$^\alpha$ (Carrera

et al., 2004).

Shell	R(Å)	Coordination number	σ^2(Å^2)	SS paths*	MS paths*
Cu −N/O	1.95	2/2	0.003	A × 2	(I,II) × 2
Cu−C/C	2.74/2.8	2/2	0.004/0.008	B × 2	V × 2
Cu−O	4.0	2	0.015	D	VI × 2

$^\alpha$ R: Coordination distances; σ^2: Debye-Waller factors or mean square displacement,

SS: Single Scattering, MS: Multiple Scattering. *See as figure 2.9.

Single Scattering Paths

A *100%* **B** *35, 70%* **C** *30 %* **D** *30 %* **AX** *15%*

Multiple Scattering Paths

I *15%* **II** *10%* **III** *5 %* **IV** *7%*

V, V' *35,70%* **VI, VI'** *30,60%*

X=N His
C Pc
O Gly
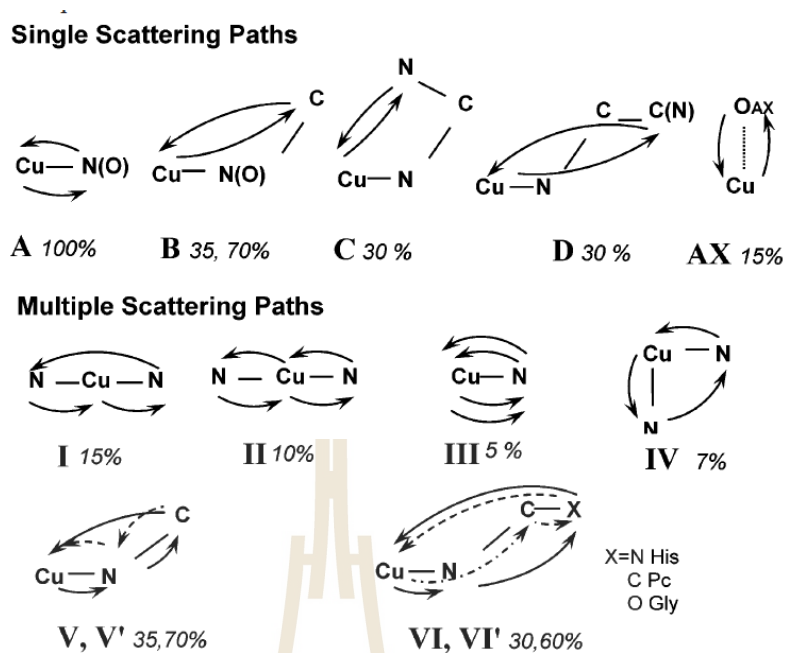
Figure 2.10 Single scattering paths and most significant multiple scattering paths included in the fits of the EXAFS spectra of the Cu(II) complexes (Carrera *et al.*, 2004).

The theoretical data of the X-ray absorption near-edge structure spectra at the Cu *K*-edge of bis-glycinatocopper(II) or Cu(II)-Glycine solution complexes was also reported by Chaboy *et al.* in 2005. The experimental Cu *K*-edge XANES spectrum, the features in the spectrum may be assigned as the following. Feature A corresponds mostly to the transition of Cu1s → 4p + ligand-metal charge-transfer (shake down transition) (Shadle *et al.*, 1993). The main transition peak is the feature B and C as shown Figure 2.11.
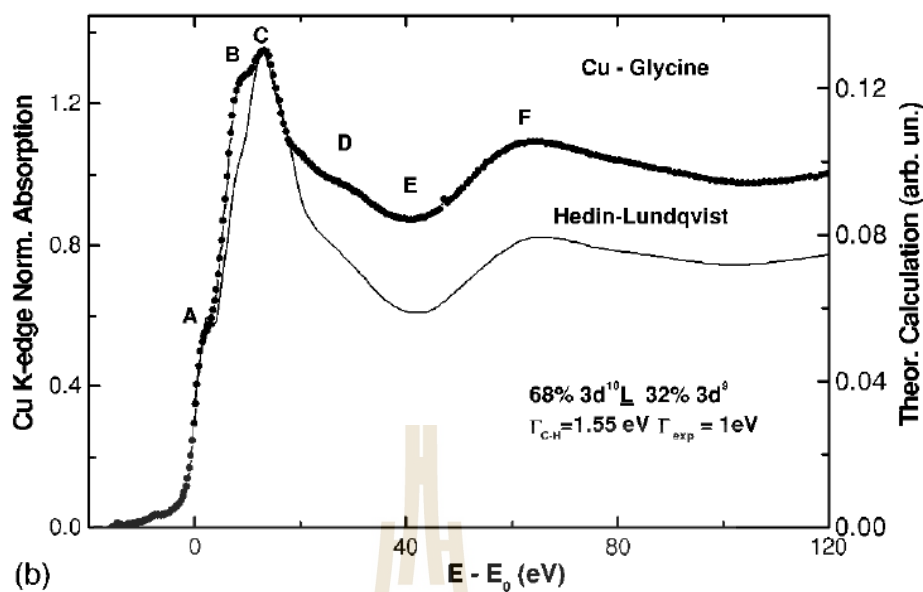
Figure 2.11 Comparison of the experimental (dot line) XANES spectrum at the Cu *K*-

edge in Cu-Glycine and the calculated spectrum (solid line) by using two

electronic configurations in the final state (Chaboy *et al.*, 2005).

2.4 X-ray absorption spectroscopy

X-ray absorption spectroscopy (XAS) technique is a powerful tool for studying

at the atomic and molecular scale, and the local structure around a selected element that

is contained within a material. XAS technique is the experiment that studies the X-ray

absorbing of the atom in the matter at a function of photon energies or X-ray energies.

The X-ray energy used in the experiment is an X-ray that can be adjusted (tunable

monochromatic) and is in the edge of the absorbing energy or close to the binding

energy of electrons (Wantana, 2012).

The X-ray absorption of an atom is caused by the decay of photons, where the

energy of photon is used to change the energy state of electron in an atom, giving rise

to the transition of the electrons in inner shells (K, L or M shell) to unoccupied state

above the Fermi level (Figure 2.12 (a)). Which causes an empty state in core-level, and the energy level in shell is used to identify the type of absorption edge i.e. K-edge or L3-edge absorption. The X-ray absorption of electron preferred to transition at K shell that excited electron from 1s shell to unoccupied state. The photon energy that causes X-ray absorption has higher than or equal to the difference K shell and unoccupied state.
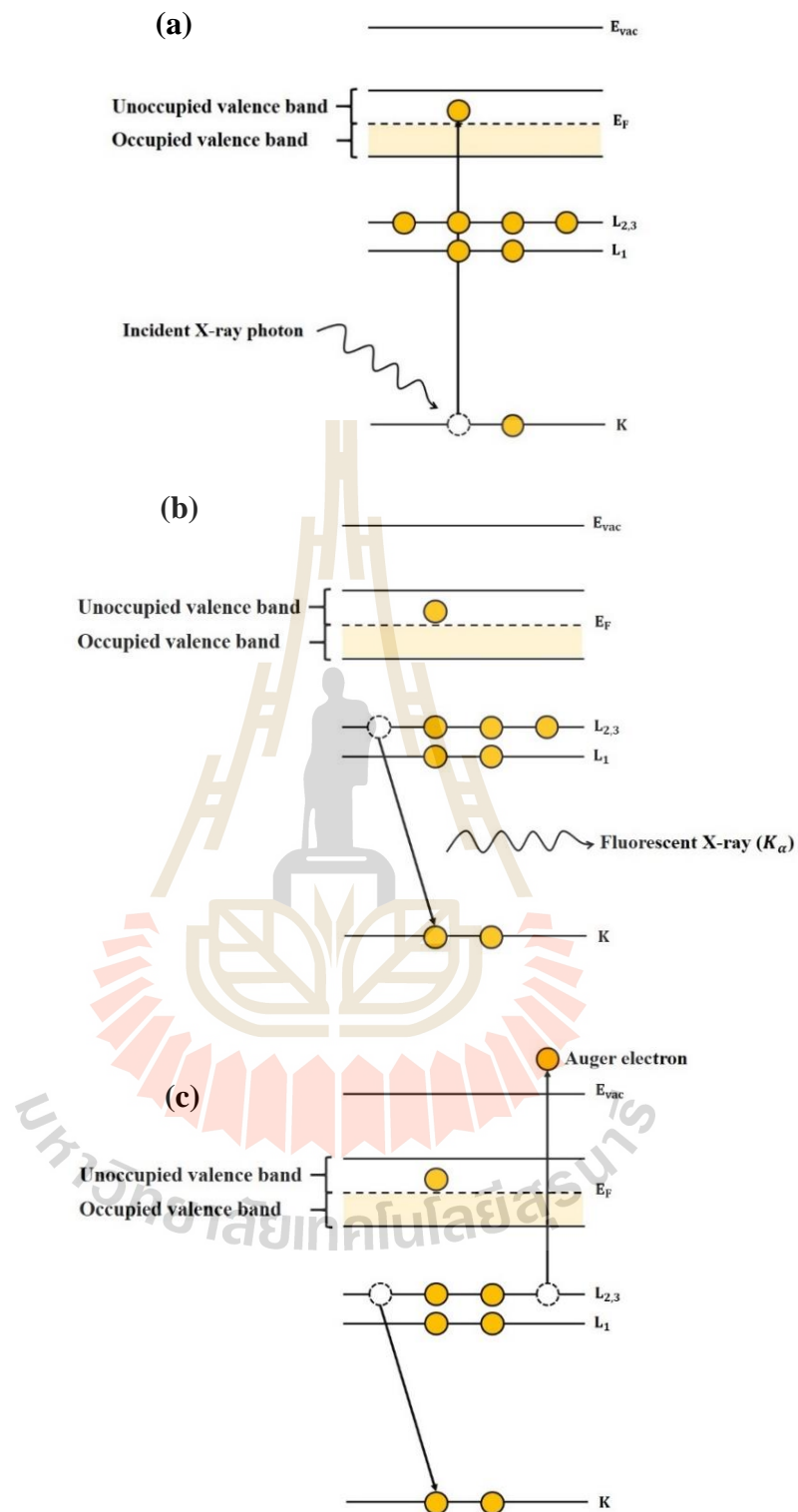
Figure 2.12 (a) Mechanism that of X-ray absorption process that gives the atom in excited state **(b)** Fluorescence X-ray emission and **(c)** Auger emission (Wantana, 2012).

For X-ray transmission, the X-ray beam of intensity passing through a sample of thickness (x) will get a reduced intensity I according to the expression

$$I_t = I_0 e^{-\mu x} \tag{2.1}$$

where I_0 is the intensity of incident X-ray beam,

I is the intensity of the beam after the beam passing through a sample,

x is the thickness of a sample,

and μ is the X-ray absorption coefficient, as shown in Figure 2.13
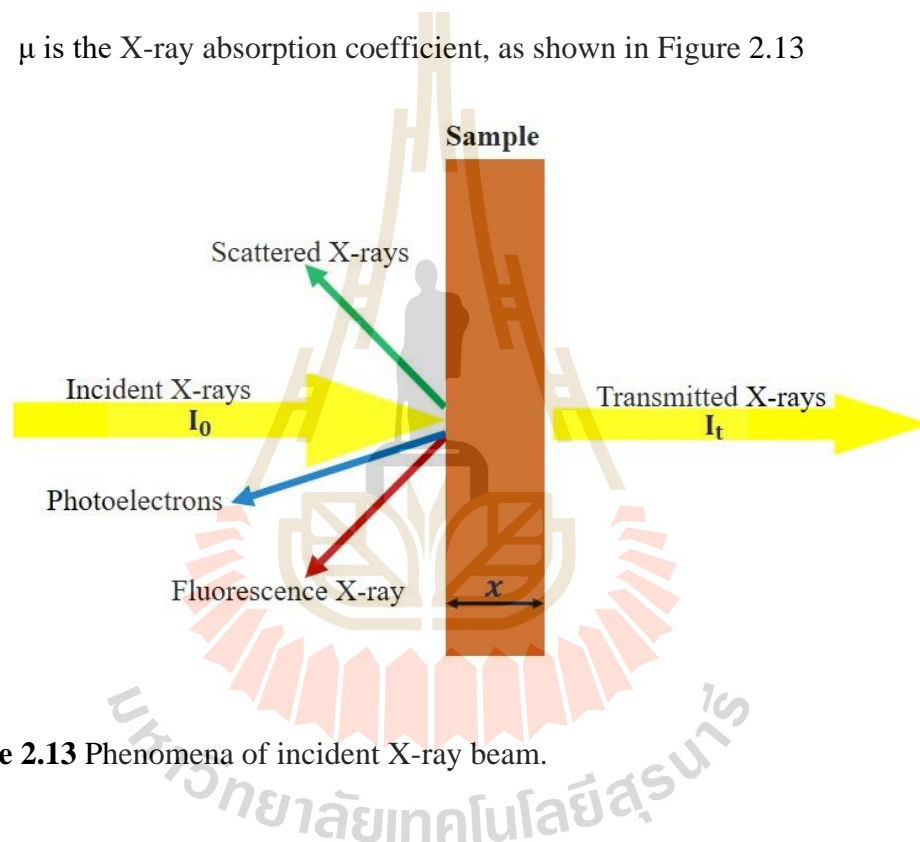
Figure 2.13 Phenomena of incident X-ray beam.

After photoelectric absorption, the excess energy of electrons is released as fluorescence X-ray emission (Figure 2.12 (b)). The X-ray energy generated by the fluorescence is equal to the difference between the energy of electron in the upper shell, such as L or M shell, and the energy state of empty shell. There are many shell of energy in the atom, fluorescence X-rays have many type such as $K_{\alpha 1}$, $K_{\alpha 2}$, $K_{\beta 1}$, and $L_{\alpha 1}$ as shown 2.14
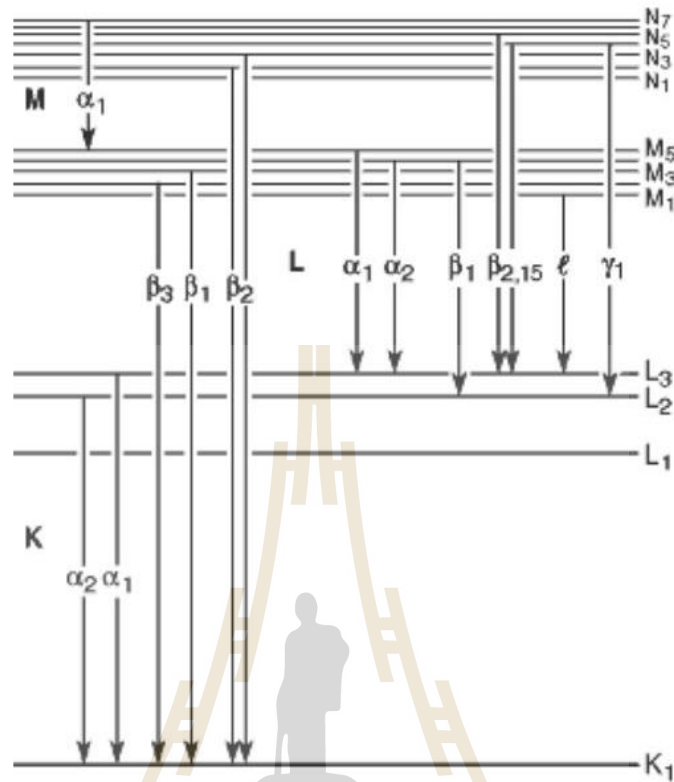
Figure 2.14 Diagram of the electronic transition to inner electron levels. (Thompson

　　　　et al., 2001)

For higher X-ray energies, the photoelectron is escaped to a free or continuum

state. The wave is created from scattering and outgoing at neighboring atoms as shown

in Figure 2.15. The scattering and outgoing of wave interfered depends on the geometry

of the absorber environment and depend on the photoelectron wavelength. The

photoelectron wavelength is inverse to the photoelectron momentum and changes with

photon energy.
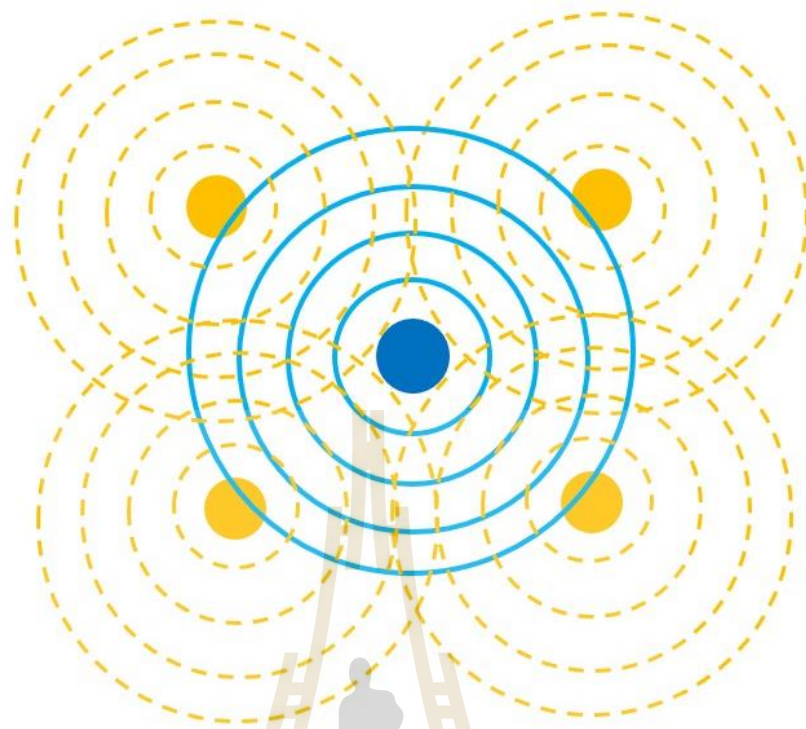
Figure 2.15 Schematic showing the absorption atom (blue) and its first nearest
neighbors (orange). An interference pattern is created by the outgoing
(solid blue lines) and reflected (dashed orange lines) photoelectron waves
(Schnohr *et al.*, 2015).

Constructive or destructive interference of scattering and outgoing waves are
affected by the absorption probability that increases or decreases, generating an energy-
dependent fine structure of the absorption coefficient ($\mu(E)$). Figure 2.16 shows the
$\mu(E)$ fine structure as a function of photon energy. Two regions are normally
distinguished, namely the X-ray absorption near edge structure (XANES) and the
extended X-ray absorption fine structure (EXAFS):

(a) A pre-edge and edge region are limited to a few eV around the edge.

(b) The structure within 30-50 eV above the edge is called XANES, information can be obtained the local electronic including geometric structure.

(c) The fine structure extending from the XANES region up to typically one thousand eV is called EXAFS. EXAFS contained information on the local structure around the absorber atom. The interpretation of EXAFS is easier than the interpretation of XANES.
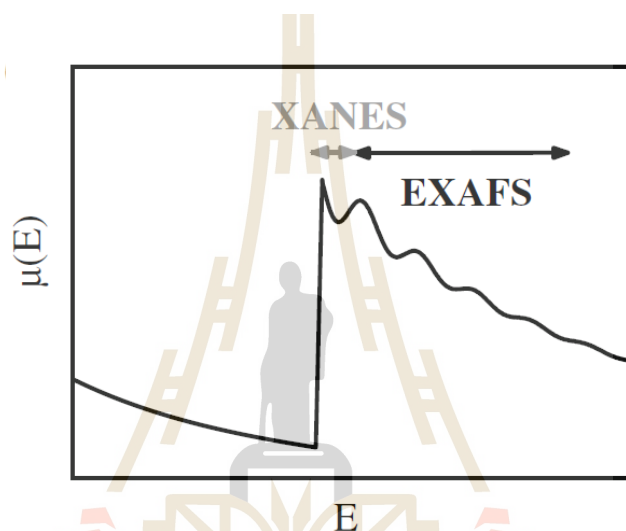
Figure 2.16 The XAS spectra divided into XANES and EXAFS region (Schnohr *et al.*, 2015).

2.4.1 X-ray Absorption near-edge structure (XANES)

The XANES region is the transition of photoelectron to unoccupied state. XANES is sensitive to the chemical bonding and exhibiting for the characteristic features of different oxidation number of the absorbing atom. The XANES features are influenced by multiple scattering effects which depend on a three-dimensional geometry of crystal structure. XANES shape of the structure is a feature that can be

used to analyze different types of chemicals (Fingerprinting), and distinguish the chemistry in the sample (Principle of component analysis).

In addition, the XANES structure also contains components of low-energy photoelectron scattering signals. Since this photoelectron can behave as a wave, it can scatter with the surrounding atoms. The scattering that occurs in the area of the XANES structure is multiple scattering and is strong because it is a photoelectron with a wavelength close to the atomic distance or the bond length. The multiple scattering also depends on the angle between the scattering atoms. Therefore, the structure XANES is useful in the study of molecular symmetry.

Calculating the wavelength of the photoelectron λ_e from the wave number k using the relationship: $k = 2\pi/\lambda_e$ The wave number of photoelectron will corresponded with X-ray energy, which follows by the rules of conservation energy,

$$k = \sqrt{\frac{2m}{\hbar^2}(E - E_0)} \qquad (2.2)$$

Where E_0 is threshold energy or ionization energy, which is the initial energy that causes the electron to move from a core energy state to a continuous free state. For an free atom or an atom that has an oxidation state equal to zero, parameter E_0 is equal to the binding energy of the electrons in the atom. Therefore seeing the absorption edge in the XANES spectrum, where the photon energy value is close to this binding energy. The atoms of the same element that are in different environments or in different oxidation states may have binding energy values which is approximately 1 eV to 15 eV. The XANES spectrum is therefore directly useful for studying the oxidation state of the atom.

2.4.2 Extended X-ray Absorption Fine Structure (EXAFS)

The photoelectron is escaped to a free or continuum state at photon energies higher than ~30 eV above the edge. EXAFS is depended on the atomic arrangement around the absorbing atom but independent of the chemical bonding. The EXAFS contains information about the coordination number, distance of atomic interaction, structural, and thermal disorder around a particular atomic species. EXAFS does not require long-range order and appropriate to a wide range of order and disorder materials.

The EXAFS is expressed in terms of the fine structure contribution. The structure factor can be described by

$$\chi(E) = \mu(E) - \mu_0(E)/\Delta\mu_0(E) \tag{2.3}$$

Where $\mu(E)$ is the absorption coefficient, $E = E_0 + \hbar^2 k^2/2m_e$ is the X-ray energy, $\mu_0(E)$ is the background absorption coefficient, and $\Delta\mu_0(E)$ is an absorption edge height (Schnohr *et al.*, 2015). Normally, structure factor can be written as a function photoelectron wave vector, $k = \sqrt{2m_e(E - E_0)/\hbar^2}$, where m_e is the electron mass and $\hbar$ is the Planck's constant. In general, $\chi(k)$ can be expressed by the classical EXAFS equation.

$$\chi(k) = \sum_j \frac{S_0^2 N_j}{k R_j^2} \left| f_j^{eff}(k, R_j) \right| \sin[2kR_j + \varphi_j(k)] e^{-2\sigma_j^2 k^2} e^{-2R_j/\lambda(k)} \tag{2.4}$$

$$\varphi_0(k,r) = \frac{e^{ik|R-r|}}{|R-r|}$$

$$\varphi_{backscatt}(k,r) = \frac{f_i^{eff}(k)e^{ik|R-r|}e^{i(\delta_i(k)-\pi/2)}}{|R-r|}$$

Neighbor atom   Absorber atom

Absorber atom   Neighbor atom

$$\varphi_{scatt}(k,r) = \frac{f_i^{eff}(k)\sin[2kR+\delta_i(k)]}{R^2}$$

Absorber atom   Neighbor atom
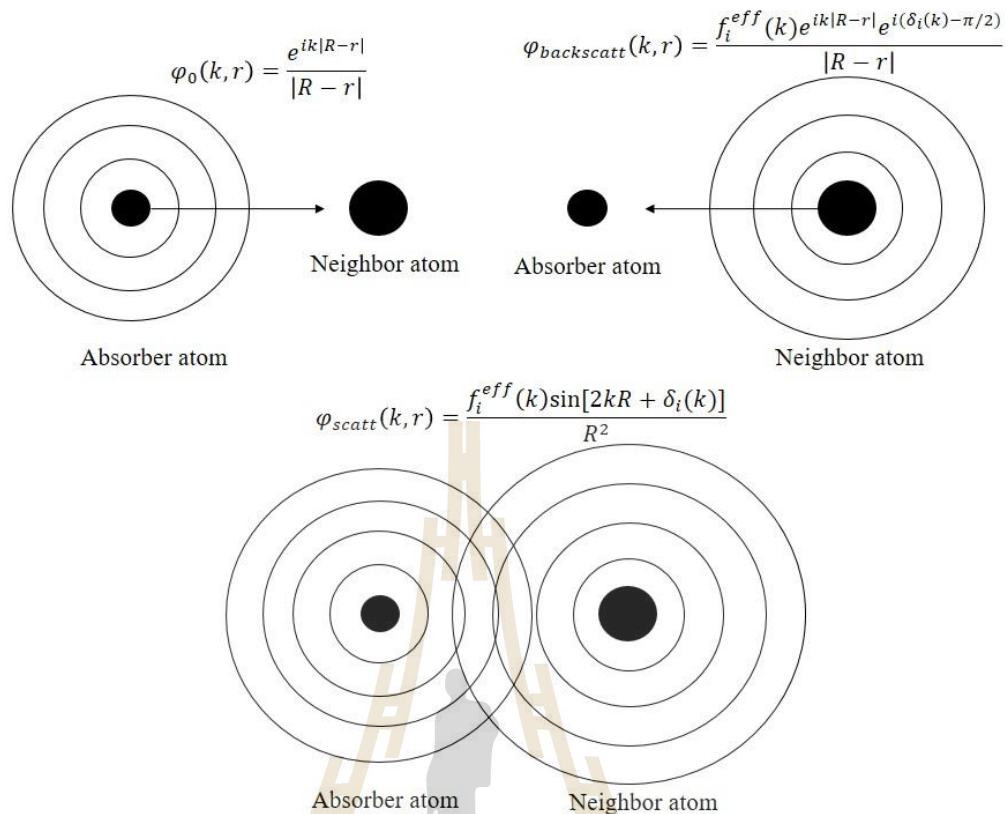
Figure 2.17 The EXAFS mechanism of photoelectron scattering (Atipong, 2014).

Fine structure contribution can be expressed a summation all scattering paths that arise from the various different paths. Therefore, paths have been grouped under the parameter j which are the same kinds of scattering atoms and the similar path length. Thus, equation (2.4) has been directly related the EXAFS signal to the structural parameters N_j, R_j, and σ_j^2 which are the coordination number, the path length, and the variation of all path lengths, respectively. S_0^2 is the amplitude reduction factor, f_j^{eff} is the curved-wave scattering amplitude, $\lambda(k)$ is the mean free path of electron, and $\varphi(k)$ accounts for the total phase shift.

The distance between core atom and backscattering atoms or the part-length change the phase contrasting with the wavelength of the photoelectron. Furthermore,

different types of surrounding atoms vary the backscattering intensity as a function of photoelectron energy. It is accepted by analysis of the the EXAFS structure, one can receive significance structural parameters surrounding the center atom.

2.5 Synchrotron radiation

Light is an electromagnetic radiation that the human eye can be detected. Electromagnetic radiation occurs the wide range of wavelengths from gamma rays to radio waves, which broad spectrum the wavelengths visible to humans occupy a very narrow band, from the red light about 700 nm to the violet light about 400 nm. The light with different wavelengths can be detected the different size of an object, the short wavelength can be detected and probed a small object. Therefore, to obtain the high-efficiency results, each wavelength was used for specific tasks.

2.5.1 Synchrotron radiation source

Synchrotron radiation is electromagnetic radiation that is emitted when charged particle moving at close to the speed of light and it is forced to change direction of motion by magnetic field. Synchrotron radiation source is a source of electromagnetic radiation usually produced by accelerating electron around the storage ring. The radiation is characterized by a continuous energy spectrum spans a wide range of wavelengths, from infrared up to hard X-rays, high intensities, strong polarized, tunable, collimated (consisting of almost parallel rays) and concentrated a small area. Modern synchrotron facilities have additional components such as bending magnets and insertion devices, placed in the straight sections between the bending magnets. The insertion devices (multi-pole wiggler, undulator, or superconducting wavelength shifter) are used for high intensity and high energy.

Figure 2.18 Schematic of synchrotron facility, (1) electron gun, (2) linear accelerator, (3) booster ring, (4) storage ring, (5) beamline, and (6) experimental station (http:// www.slri.or.th).

2.5.2 Synchrotron Light Research Institute source

The synchrotron light research institute (SLRI) source is an electron accelerator complex consisting of a 40 MeV linear accelerator (LINAC), a 1 GeV booster synchrotron (SYN), and a 1.2 GeV electron storage ring (STR). The electrons are produced by an electron gun then accelerated by 2856 MHz high power microwave in the linear accelerator. The 40 MeV electrons are transported by the low energy beam transport line (LBT) to the booster synchrotron and accelerated to 1 GeV by 118 MHz Ratio Frequency wave in the RF cavity of the booster synchrotron. The 1 GeV electrons are transported by the high energy beam transport line (HBT) to the storage ring and further accelerated to 1.2 GeV. The outline of components showed in Figure 2.19.

Figure 2.19 The component of synchrotron radiation source of SLRI (http://www.slri.or.th).

A 1.2 GeV electron storage is stored in the vacuum tube of storage ring that has circumference 81.3 meters. When the electrons are curved in a magnetic field of storage ring, the synchrotron radiation was emitted, as shown in Figure 2.20.
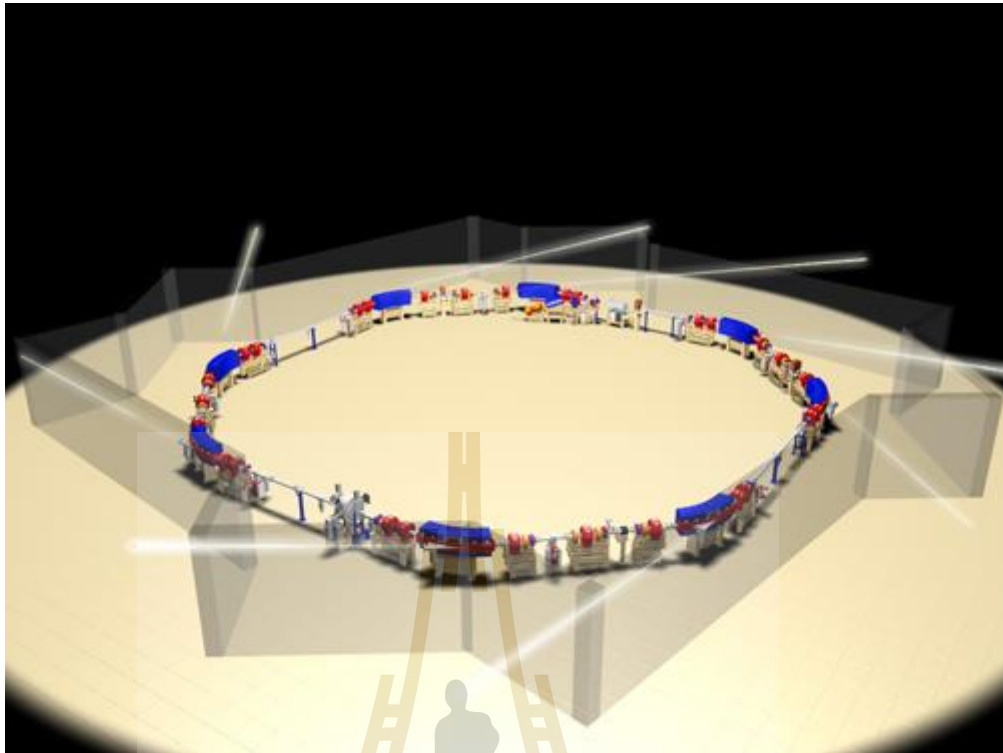
Figure 2.20 The emitting of synchrotron radiation from bending magnet (http://www.slri.or.th).

2.5.3 Optical element of Beamline 1.1W

Beamline 1.1W used multi-pole wiggler in the insertion devices section for giving high energy. The BL1.1W has the 3 optical elements (Figure 2.21) to accommodate both scattering and spectroscopy techniques. The collimating mirror is used to obtain the vertical collimation beam. The double crystal monochromator (DCM) is used to select the energy to achieve the monochromatic beam with 10^{-4} energy resolution required to the spectroscopy technique. The toroidal focusing mirror is used to reduce the beam size and adjust symmetry of beam profile suitable to the scattering technique.
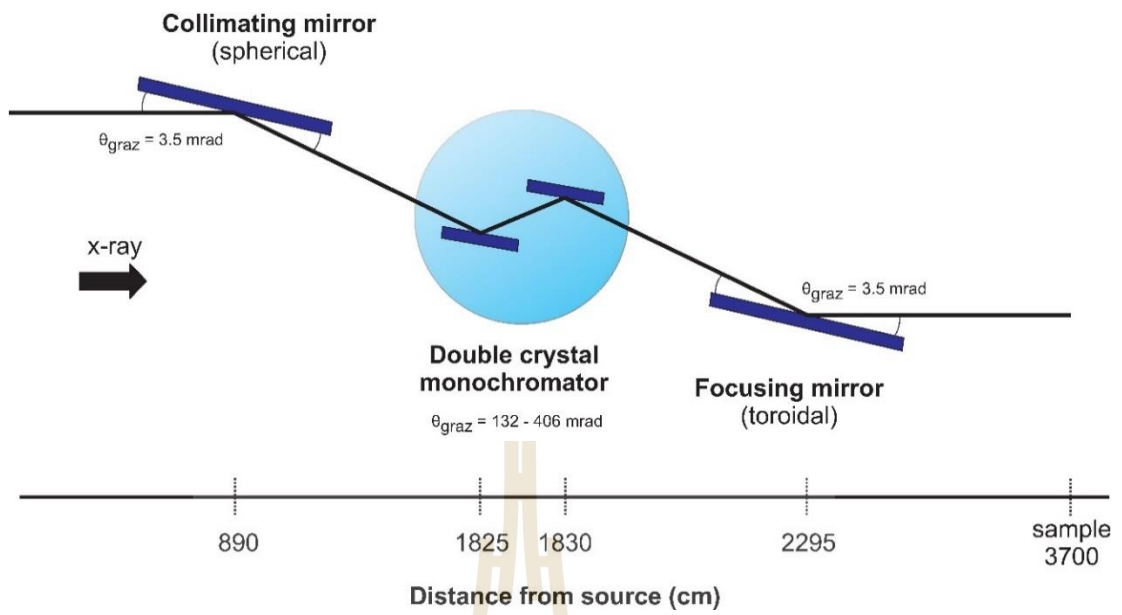
Figure 2.21 Three main optical elements at BL1.1W; a collimating mirror, a double

crystal monochromator, and a focusing mirror (http:// www.slri.or.th).

CHAPTER III

MATERIALS AND METHODS

3.1 Preparation of solutions

Copper (II) chloride dihydrate ($CuCl_2 \cdot 2H_2O$) powder and glycine powder available in commercial market were purchased to prepared a Copper (II) chloride and glycine solution. A stock solution of 2.5 M copper (II) chloride was prepared by dissolving 10.66 g of $CuCl_2 \cdot 2H_2O$ powder in deionized water and the volume of solution was adjusted in a 25 mL volumetric flask. The solution of 0.5M, 0.25M and 1.5mM Cu(II) were obtained from dilutes of 2.5 M Cu(II) with appropriate volume of deionized water at 1000 μL as shown in Table 3.1. A stock solution of 2.5M glycine was prepared by dissolving 4.69 g of glycine powder in deionized water to produce 25 mL solution.

Table 3.1 The volume of Copper (II) chloride solution by dilution of deionized water.

Concentration	Volume (μL)	
	Copper(II) chloride solution	Deionized water
0.5M	200	800
0.25 M	100	900
1.5 mM	6	994

Cu(II):Glycine solution was carried out by mix the solution of copper (II) chloride and glycine in 5 ratios (1:1, 1:2, 1:3, 1:4, and 1:5). Concentration of Cu(II) solutions were fixed at 0.5 M, 0.25 M, and 1.5 mM as shown in Table 3.2.

Table 3.2 The volume ratio of glycine solution to use in experiment.

Ratios	Volume of glycine (total volume = 1000 μL)					
	0.5 M Cu(II):Glycine		0.25 M Cu(II):Glycine		1.5 mM Cu(II):Glycine	
	Glycine*	DI water	Glycine*	DI water	Glycine*	DI water
1:1	200	800	100	900	1.5	998.5
1:2	400	600	200	800	-	-
1:3	600	400	300	700	4.5	995.5
1:4	800	200	400	600	-	-
1:5	1000	0	500	500	7.5	992.5

* Dilution from 2.5 M of glycine solution, ** Dilution from 1.0 M of glycine solution

3.2 X-ray absorption spectroscopy setup

3.2.1 X-ray absorption spectroscopy experiment

X-ray absorption spectroscopy (XAS) experiment is usually performed at synchrotron radiation source, which provide high intensity, continuous, and tunable light source.

3.2.1.1 XAS in transmission mode of measurements

The transmission mode is the simplest type of X-ray absorption spectroscopy (XAS) measurement. In a transmission experiment, the intensity of the X-ray beam is

measured before and after the sample. The intensity of transmitted photons (I_t) detected

by the second ion chamber is given by

$$I_t = I_0 e^{-\mu_t(x)} \tag{3.1}$$

Where *x* is the thickness of the sample, *x* is usually ignored as it is eliminated

when the XAS is extracted. And μ_t is the total absorption coefficient.

$$\mu_t(x) = -\ln(I_t/I_0) \tag{3.2}$$

The intensity of the X-ray beam is measured using ionization detectors. These

detectors consist of a chamber filled with a gas mixture. The X-ray beam passes through

window at each of the chamber between two oppositely-charged plated. The current

passing between the plates is proportional to the X-ray intensity (Lee *et al*.,1981).
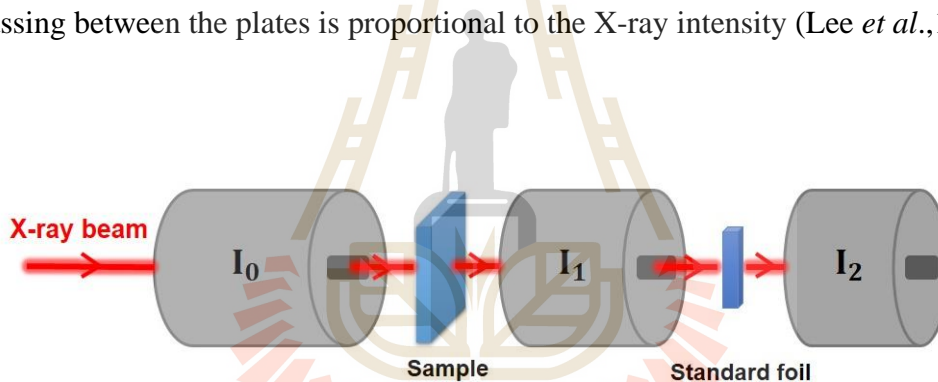
Figure 3.1 Typical for a transmission XAS experiment. I_0, I_1, and I_2 are ionization

detectors. A transmission experiment requires only I_0 and I_1. The additional

of I_2 permits the XAS of a standard foil such as a metal foil to be measured.

The schematic diagram of a transmission-mode XAS experiment is shown in

Figure 3.1. The last detector is added to allow the concurrent measurements of the XAS

from a standard foil. This standard spectrum is used for accurate energy calibration.

3.2.1.2 XAS in fluorescence mode of measurements

Fluorescence experiments are much more sensitive than transmission, and typically used with samples in which the absorbing atom is diluted (Lee *et al*., 1981). In a fluorescence experiment, the absorption of the sample is measured by monitoring the intensity of the X-ray fluorescence produced when higher-shell electrons relax into the hole left by the photoelectron. The total absorption coefficient is:

$$\mu_x = C(I_f/I_0) \tag{3.3}$$

Where C is approximately constant and I_f is the intensity of the X-ray fluorescence.

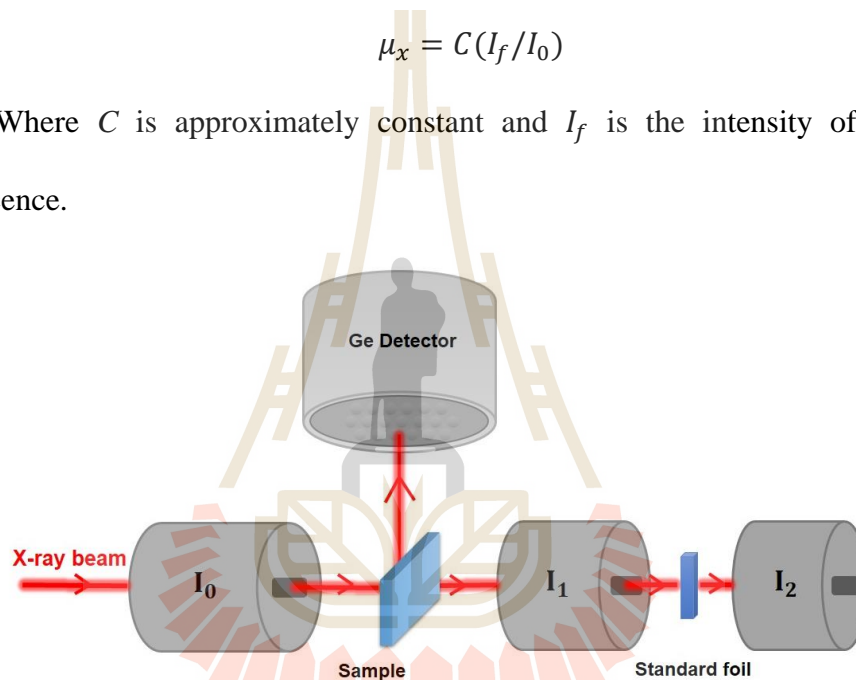**Figure 3.2** Typical fluorescence-mode XAS experimental setup.

XAS experiment in fluorescent mode is also shown in Figure 3.2. The florescence signals are detected by the fluorescence detector. The sample is commonly oriented at 45° to the beam and the fluorescence detector placed at 90°. Because the X-ray does not have to pass through the fluorescence detector. This experiment requires only I_0 and I_f.
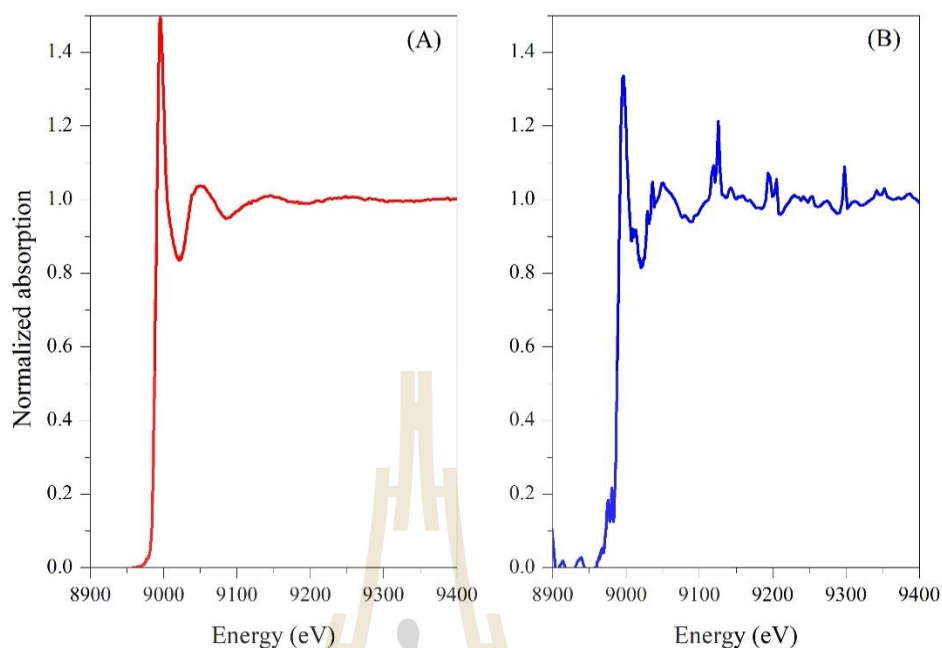
Figure 3.3 Comparison XAS spectrum of fluorescence mode (A) and transmission mode (B) for the low concentration.

At low concentrations, XAS measurements are normally measured in the fluorescence mode. Because the spectrum from the measurement shows good signal to noise ratio, as shown in Figure 3.3.

3.2.2 X-ray absorption spectroscopy experiment setup at BL 1.1W

The Cu K-edge absorption spectra of Cu(II):Glycine aqueous solutions were measured at the beamline 1.1W of the Synchrotron Light Research Institute (SLRI), Nakhon Ratchasima, Thailand. The SLRI storage ring was operated at an energy of 1.2 GeV, with the electron beam current between 80-140 mA. The beamline provides hard X-rays with photon energy between 4 to 18 keV. The X-ray source of this beamline is a 2.2 Tesla Multipole Wiggler. The synchrotron radiation was monochromatized by a

commercial double-crystal X-ray monochromator equipped with Si(111) crystals. Mixture solutions were kept in plastic bag with dimension of 4cm×5cm. All XANES and EXAFS spectra were measured at room temperature and atmosphere pressure. The photon energy was calibrated using a copper foil as a reference. XANES spectra were measured in the transmission mode using ionization chambers as detectors for high copper concentration solutions. Ionization chambers were filled with a 20% of Ar/He mixture and optimized for the beam intensity in I_0 and filled with a 40% of Ar/He mixture in I_1 and I_2. Fluorescence mode using a Canberra 19-element Germanium solid state detector was preferred for low concentration solutions. The scanning photon energy is used with energy step of 0.2 eV for XANES spectra and $0.05k$ eV for EXAFS spectra. To improve the signal-to-noise ratio, three scans were recorded and averaged, the experimental setup showed in Figure 3.4.
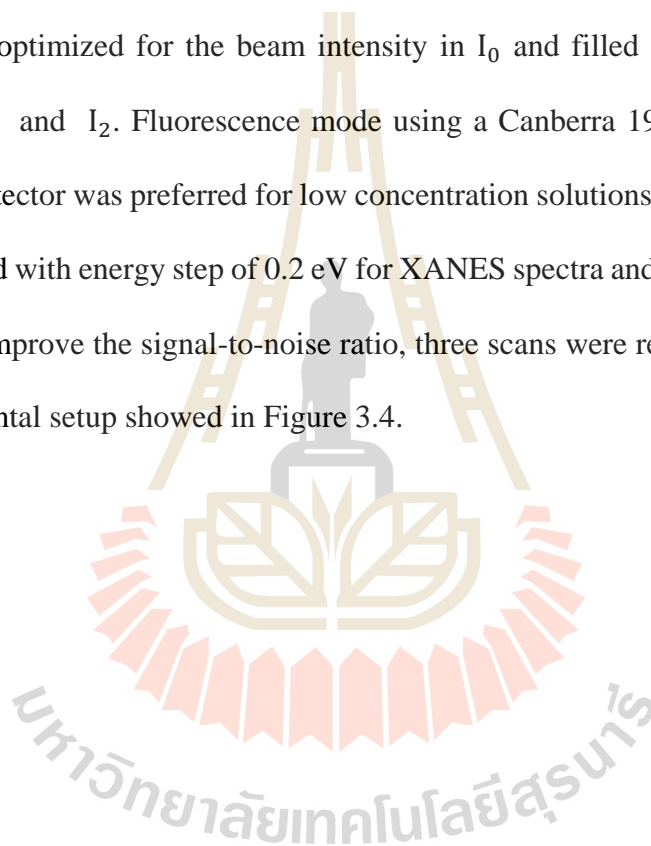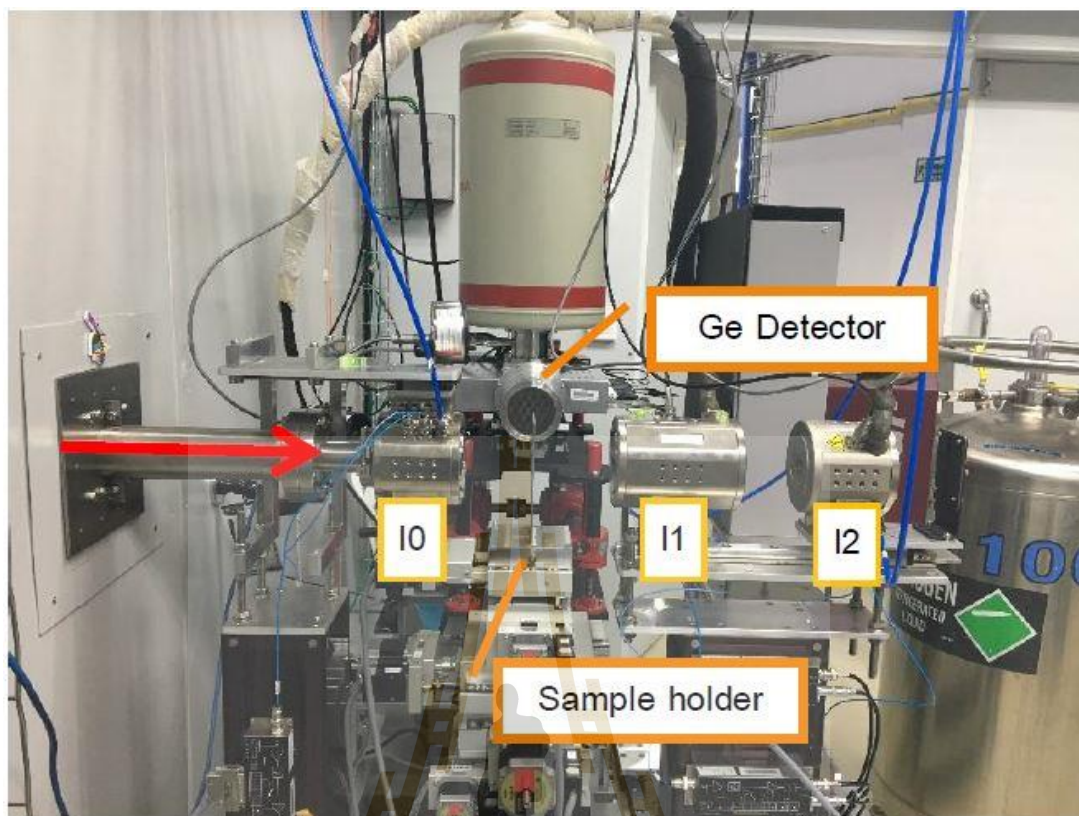
Figure 3.4 Schematic of the setup for XAS measurements in transmission mode and

fluorescence mode at BL 1.1W of SLRI, Thailand.

CHAPTER IV

RESULTS AND DISCUSSION

Investigations of all aqueous solutions have been carried out using X-ray absorption spectroscopy. The obtained spectra are compared with the XAS spectra from Cu foil (0 oxidation state), Cu_2O (+1 oxidation state), CuO (+2 oxidation state) and $CuCl_2$ (+2 oxidation state) as shown in Figure 4.1. For clarity, the absorption spectra are normalized and offset vertically by 0.2. Interestingly, the absorption spectrum of the mixed solution is rather close in shape to the one of CuO. From the Cu(II):Glycine and CuO spectra, we observed absorption features: (i) a pre-edge peak (A) at ($\Delta E \sim 7.8$ eV); (ii) a split main absorption line (B $\sim$ 14.6 eV; C $\sim$ 19.6 eV); (iii) shoulderlike feature (D) at the high-energy side of the C peak; and finally, (iv) a deep minimum (E $\sim$ 45 eV). In particular, A peak corresponds mostly to the transition Cu 1s→4p+LMCT shakedown at $\sim$ 8987 eV, and B and C are the main transitions Cu 1s→4p (Shadle *et al*., 1993), the B peak is depressed as compared to C peak. In Cu(II):Glycine complexes, the first local coordination shell around copper has been formed by 2 nitrogen and 2 oxygen atoms (Chaboy *et al*., 2005). The main absorption line of the spitted B and C peaks is significantly different for the four complexes.
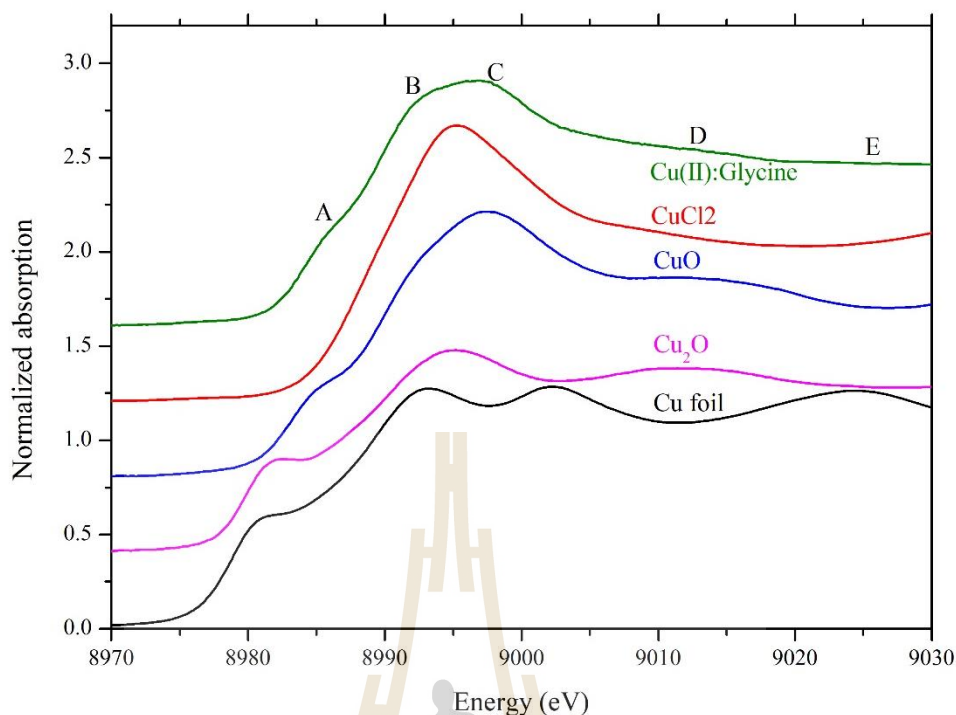
Figure 4.1 Cu K-edge XANES spectra of Cu foil, Cu_2O, and CuO standard samples
and $CuCl_2$ and Cu(II):Glycine sample solutions.

The absorption edge energy of $CuCl_2$ and CuO represented by the oxidation
state: +2. The absorption edge energy of $CuCl_2$ is 8990 eV and CuO is 8984 eV. Due
to the electronegativity of Cl atom more than O atom which is the electron of $CuCl_2$
also used more the energy from the core level to an unoccupied state.

4.1 XANES spectra analysis

Experimental XANES spectra of 0.25 M copper chloride aqueous solution,
either pure or mixed with glycine aqueous solutions for concentrations ranging from
0.25 M to 1.25 M, are shown in Figure 4.2. When the concentration of glycine aqueous
solution increases, the amplitude of white line decreased. Therefore, the coordination
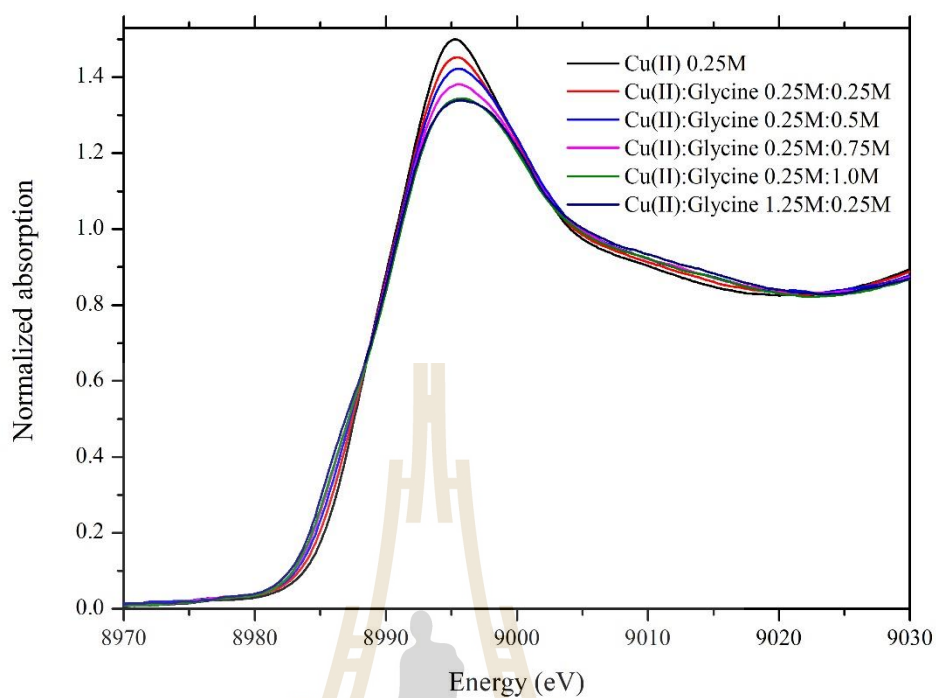number of oxygen around copper decreased with a high concentration of glycine.

Figure 4.2 Cu K-edge XANES spectra of Cu(II):Glycine in 0.25M:0.25M to 0.25M:1.25M.

A very similar trend is observed Figure 4.3, corresponding to solutions having a concentration of copper of 0.5 M, with concentration of glycine ranging from 0.5 M to 2.5 M.
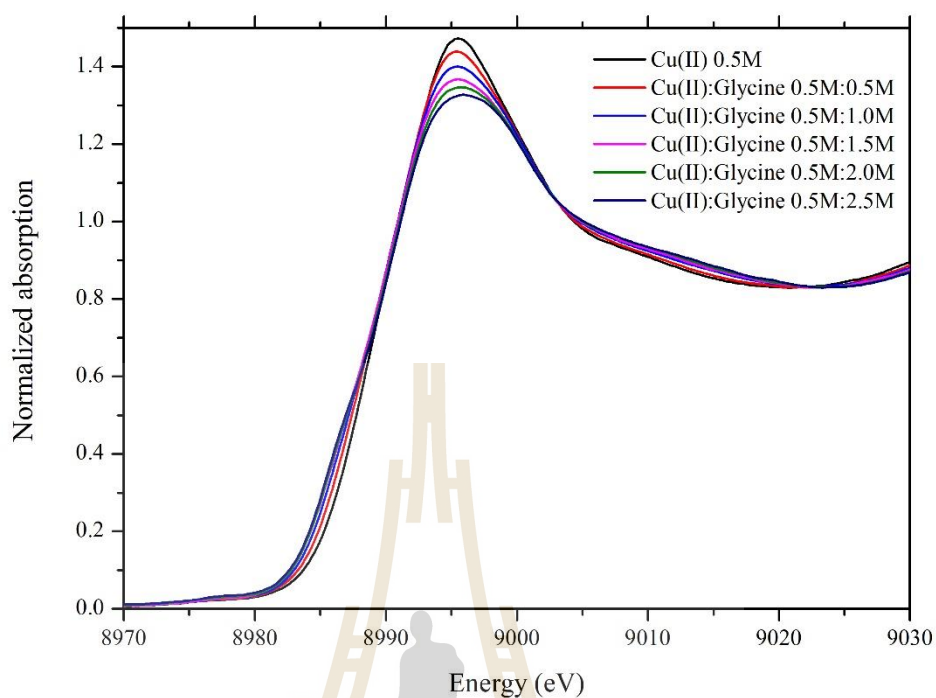
Figure 4.3 Cu K-edge XANES spectra of Cu(II):Glycine in 0.5M:0.5M to 0.5M:2.5M.

Figure 4.4 showed the Cu K-edge absorption spectra for Cu(II):Glycine with solution 1.5mM:1.5mM, 1.5mM:4.5mM and 1.5mM:7.5mM concentration ratios that measured by fluorescence mode. The amplitude of these spectra gradually decreases with increasing the concentration of glycine.
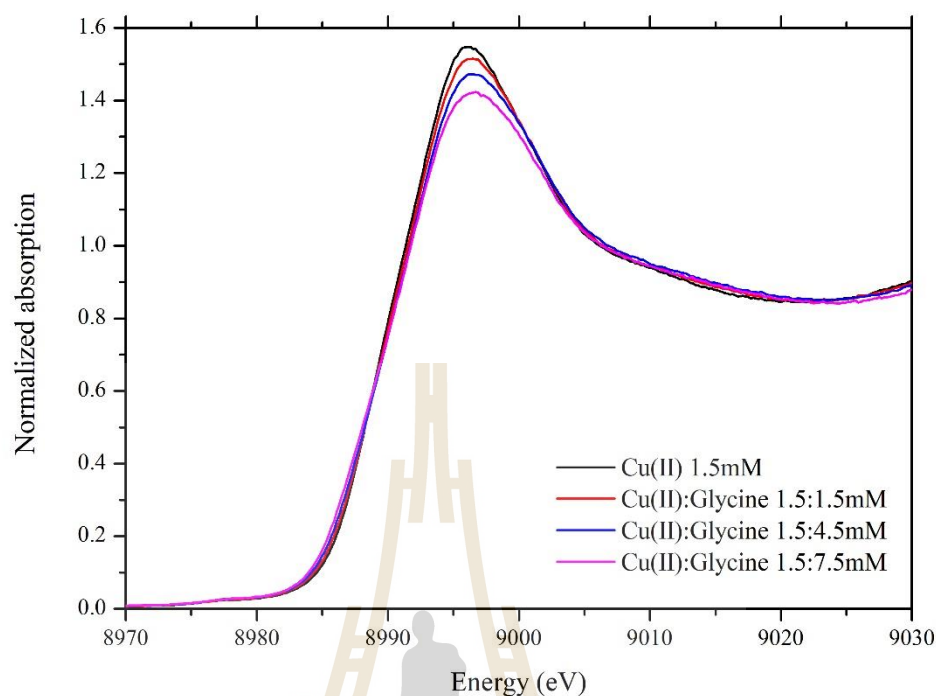
Figure 4.4 Cu K-edge XANES spectra of Cu(II):Glycine in 1.5mM:1.5mM to 1.5mM:7.5mM.

Figure 4.5 showed the consistent absorption feature changed when increasing the molar ratio of Cu(II):Glycine, likewise observed in previous experiments. Moreover, this experiment clearly reveals the structural differentiation occurred. When adjusting the pH value of 5.0 throughout the study, XANES spectrum becomes broader with the increment of molar ratio of Cu(II):Glycine from 1.5 mM:1.5 mM to 1.5 mM:7.5 mM, due to the occurrence of the split main absorption line (B and C peaks) of copper complex with glycine. Moreover, these structural features are found in all previous results shown but the similarity of B and C peaks are clearly observed with the adjustment of the pH 5.0. Since the major species formed is $CuGly_2$, this

experimental spectrum is significantly promoted. The shoulderlike feature (D peak) and the deep minimum (E peak) are apparently observed as well.
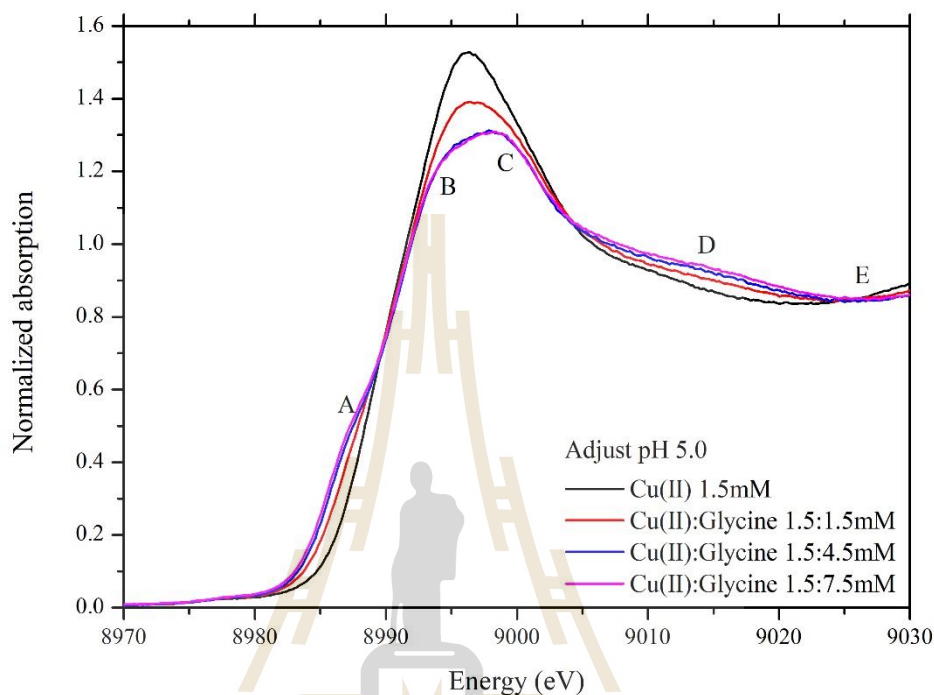

Figure 4.5 Cu *K*-edge XANES spectra of Cu(II):Glycine in 1.5mM:1.5mM to 1.5mM:7.5mM with adjusted the pH value of 5.0.

4.2 EXAFS spectra analysis

The EXAFS spectra were processed and information on local structure of Cu atom was obtained via fitting with Cu(II):Glycine model in ARTEMIS program. To process and enhance the EXAFS with the high *k* region, the plot $k^3\chi(k)$ is considered and windowed using a Hanning window *W(k)*.

Figure 4.6 showed Fourier Transform of Cu(II) standard at concentration of 0.5 M, 0.25 M, and 1.5 mM, that have been calculated in the interval k = 3-12 Å^{-1} for

solutions. The first peak was observed nonphase-shift-corrected FT at 1.5 Å that identified Cu-O from water molecules. Moreover, the second shell of concentration 1.5 mM and 0.5 M are similar. In contrast to the concentration of 0.25 M, the second shell has a different feature, because the pH of $CuCl_2$ solution at the concentration of 0.25 M exceeds the value of pK_{a1}, the structure of the $CuCl_2$ solution at a concentration of 0.25 M is different.
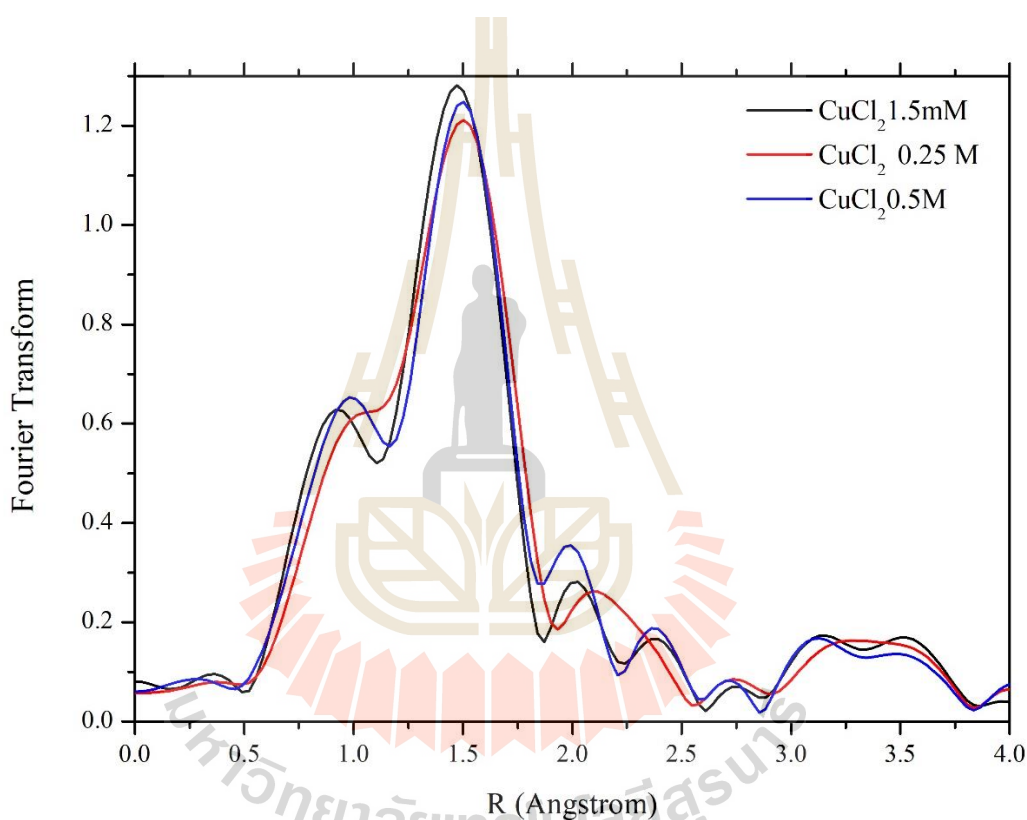

Figure 4.6 Fourier transforms of Cu(II) standard at 0.5 M, 0.25 M and 1.5 mM.

Figure 4.8 shown Fourier transforms (FTs) of Cu(II):Glycine with copper concentration 0.25M, FTs have been calculated in the interval k = 3-9 Å^{-1} (Figure 4.7). The first peak was observed at about 1.5 Å and the second peak was found at about 2.3 Å. Two peaks previously reported in the nonphase-shift-corrected FT at 1.6 Å and 2.4 Å were identified as the Cu-glycine and Cu-O$_{ax}$, thus mentioning between that of copper

and water oxygen atom at the axial position (D'angelo, 1998). The intensity variation

of second peak relied on the glycine molecule coordinated to copper and the positions
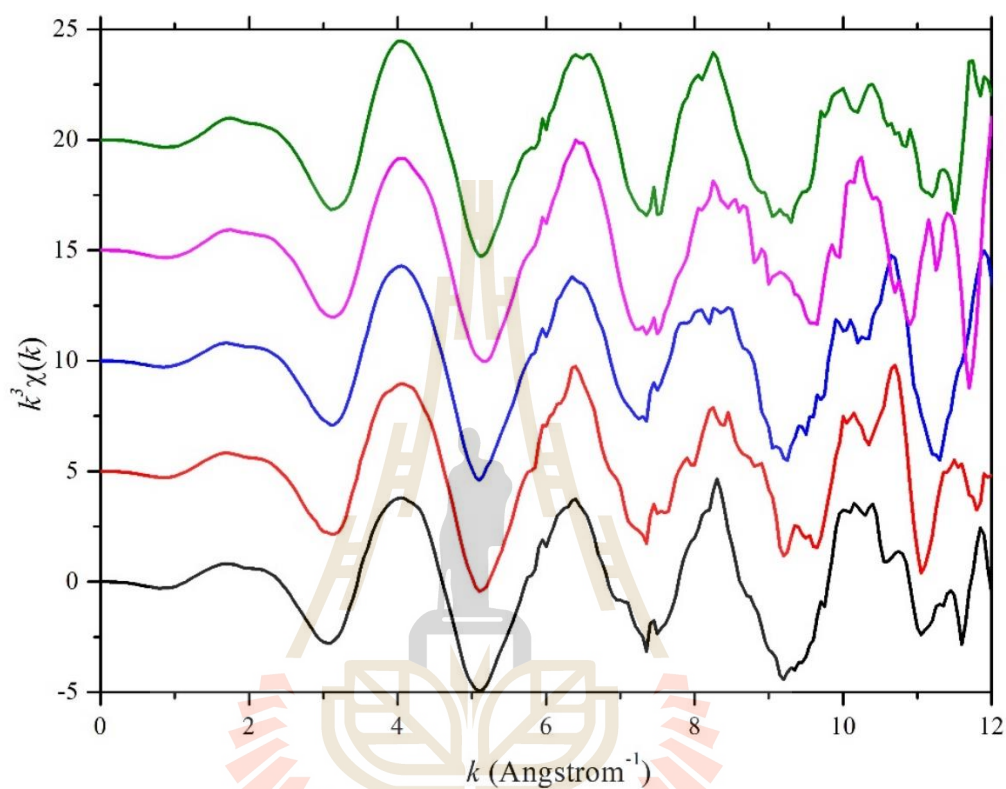
of two water molecules.

Figure 4.7 Raw data EXAFS data, k^3-weighted of Cu(II):Glycine of 0.25M:0.25M

(black line), 0.25M:0.5M (red line), 0.25M:0.75mM (blue line),

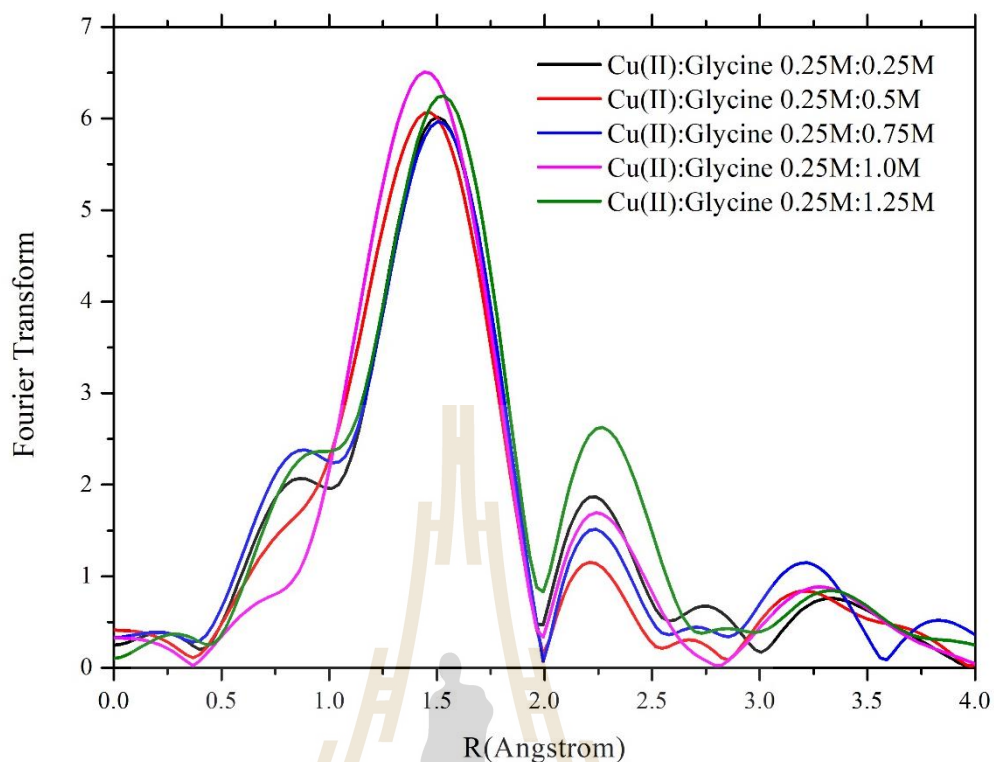0.25M:1.0M (pink line), and 0.25M:1.25M (green line).

Figure 4.8 Fourier transforms of Cu(II):Glycine in 0.25M:0.25M to 0.25M:1.25M.

Two of five mixture have pH values below 2.4, suggesting that dominate copper species is $CuGlyH^{2+}$. For the solutions Cu(II):Glycine from 0.25M:0.75M to 0.25M:1.25M, the pH values are between 2.40 to 2.51, shown in the table 4.1. Where pH values higher than pK_{a1} of the carboxylic group of glycine, the zwitterionic from $H_3N^+CH_2CO_2^-$ defined as GlyH should be dominant and the concentration of the $CuGly^+$ complex should increase.

Table 4.1 The parameters of various molar ratios of 0.25M Cu(II):Glycine.

The concentration of Cu(II):Glycine	pH value
Pure Cu(II) 0.25M:0M	3.05
0.25M:0.25M	2.09
0.25M:0.5M	2.22
0.25M:0.75M	2.40
0.25M:1.0M	2.42
0.25M:1.25M	2.51

Figure 4.9 showed Fourier transform of Cu(II):Glycine for a copper concentration 0.5M, with glycine concentration ranging from 0.5 M to 2.5 M, the pH is measured between 1.90 to 2.36 (shown in table 4.2). For the pH values less than 2.4, the $GlyH^{2+}$ species should be the dominant one, leading to the main complex $CuGlyH^{2+}$. Therefore, the first peak from EXAFS data analysis shows a gradual amplitude increase when increasing the concentration of glycine from 0.5 M to 2.5 M.
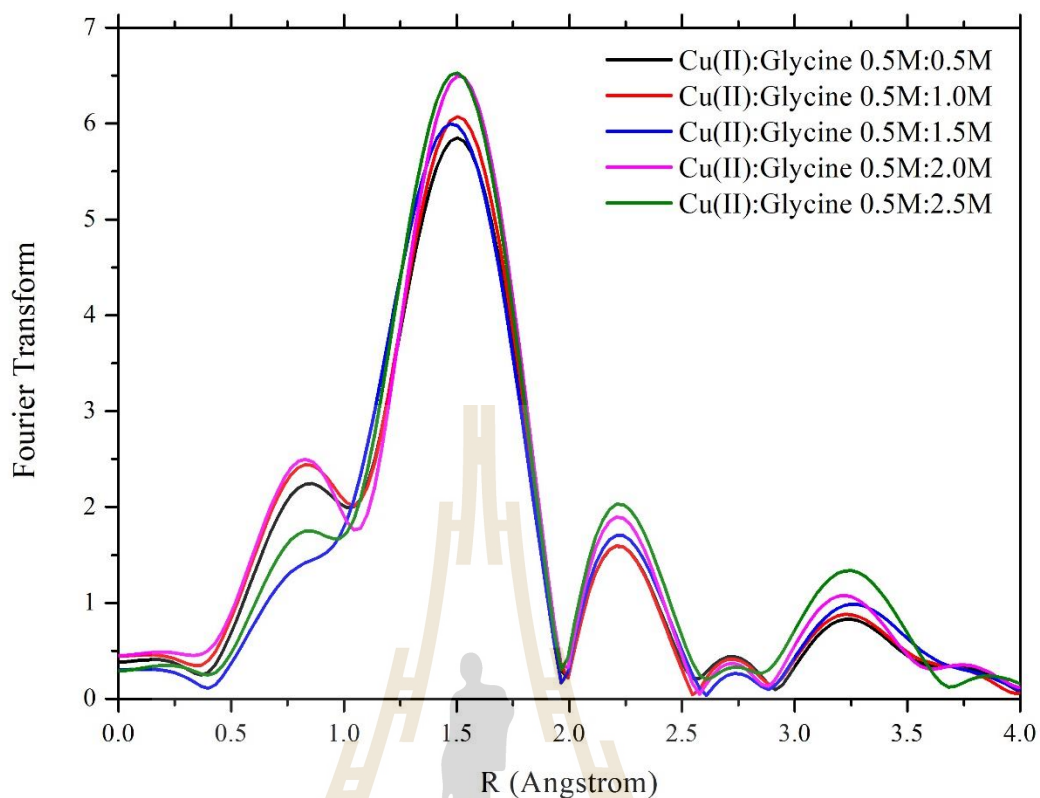
Figure 4.9 Fourier transforms of Cu(II):Glycine in 0.5M:0.5M to 0.5M:2.5M.

Table 4.2 The parameters of various molar ratios of 0.5M Cu(II):Glycine.

The concentration of Cu(II):Glycine	pH value
Pure Cu(II) 0.5M:0M	2.50
0.5M:0.5M	1.85
0.5M:1.0M	1.95
0.5M:1.5M	2.08
0.5M:2.0M	2.20
0.5M:2.5M	2.34

Therefore, when the concentration of glycine solution increases that affected the increment molecule of glycine as the pH value stays in the range of pK_{a1}= 2.35. When the pH value more than 2.35, the copper species changes. Moreover, at high concentrations (0.25 M and 0.5 M) are complicated to indicating for the structure of Cu(II):Glycine solution. We can specify the local structure of Cu(II):Glycine at the only the first shell.

Figure 4.11 showed the EXAFS spectra of Cu(II):Glycine of copper concentration of 1.5mM. The FT analysis has been carried out in the interval k = 3-9 Å^{-1} (Figure 4.10), the first shell does not directly correlate with increment of molar ratio of Cu(II):Glycine. Due to the pH value of these solutions have 2.87, 2.90, and 2.98 respectively, which associates to the copper species formed.
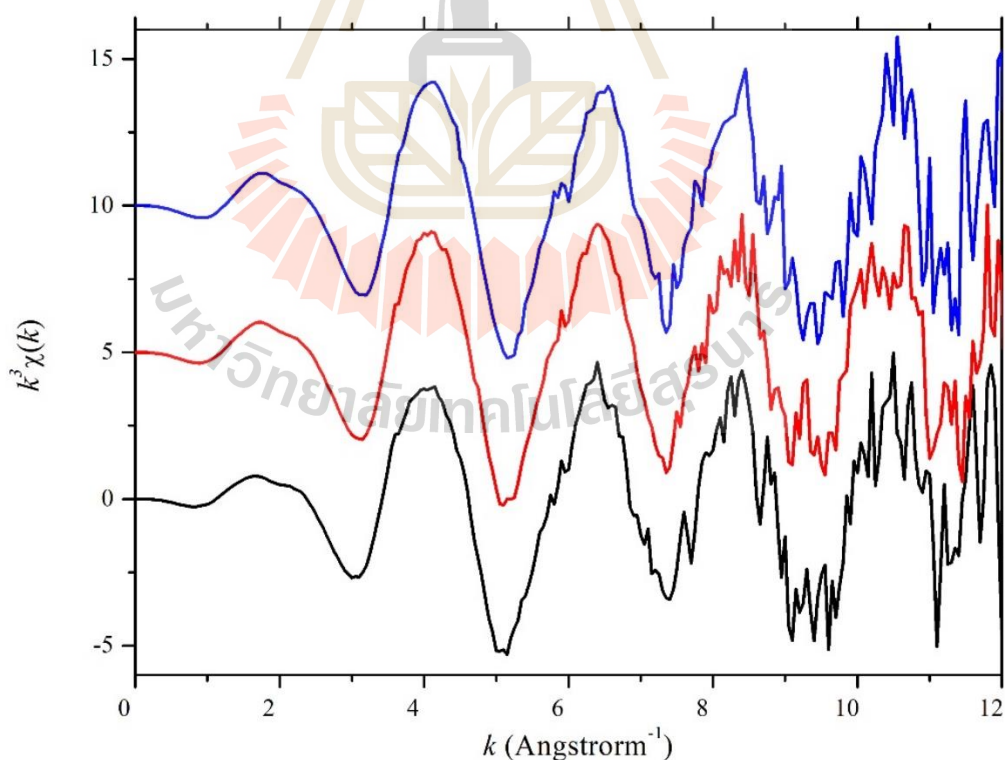

Figure 4.10 Raw data EXAFS data, k^3-weighted of Cu(II):Glycine of 1.5mM:1.5mM (red line), 1.5mM:4.5mM (blue line), and 1.5mM:7.5mM (black line).
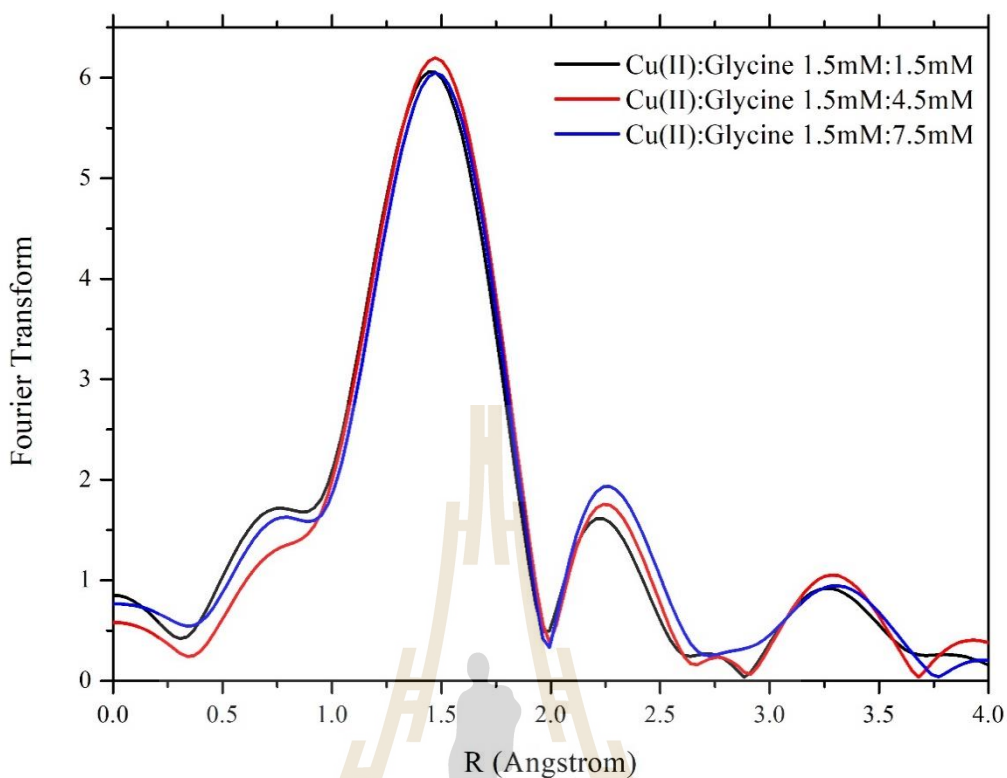
Figure 4.11 Fourier transforms of Cu(II):Glycine in 1.5mM:1.5mM to 1.5mM:7.5mM.

Figure 4.13 showed Fourier transform of Cu(II):Glycine at low concentration (the copper concentration 1.5mM) with adjusted the pH value to 5.0. The EXAFS spectra have been performed in the range k = 3-9 Å^{-1} as shown in the Figure 4.12. The first peak in the nonphase-shift-corrected FT at ~1.5 Å is accounted for the Cu-glycine signal and the second peak in FT at 2.4 Å is accounted for the Cu-O$_{ax}$ signal.
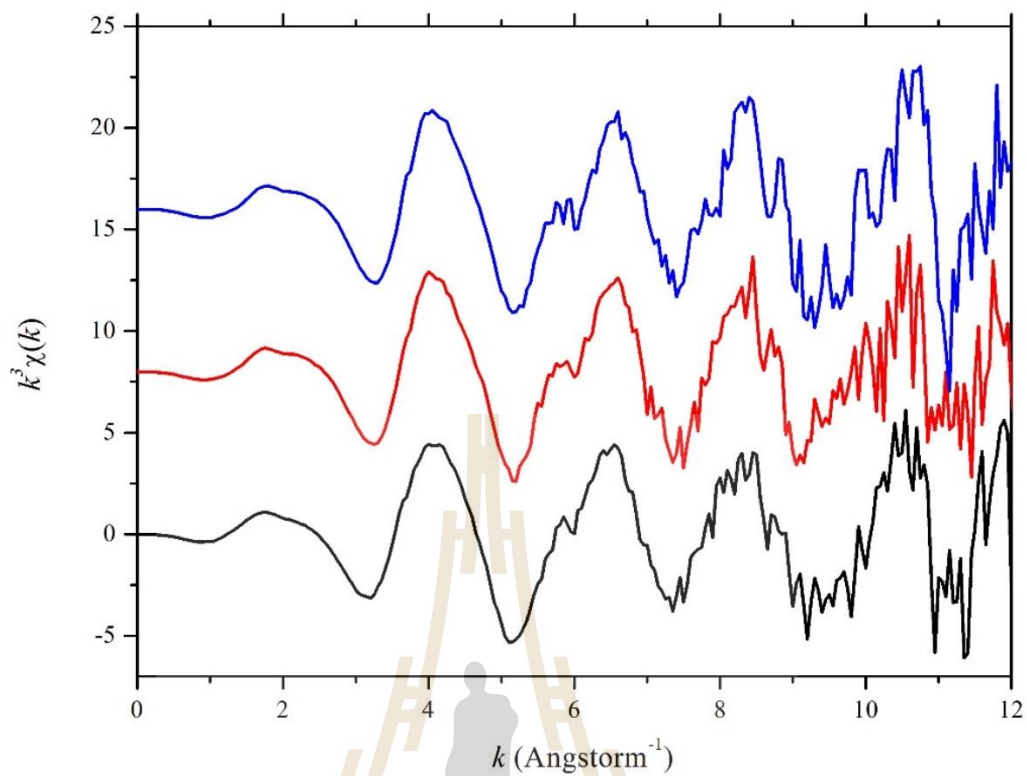
Figure 4.12 Raw data EXAFS data, k^3-weighted of Cu(II):Glycine of 1.5mM:1.5mM

(red line), 1.5mM:4.5mM (blue line), and 1.5mM:7.5mM (black line) with
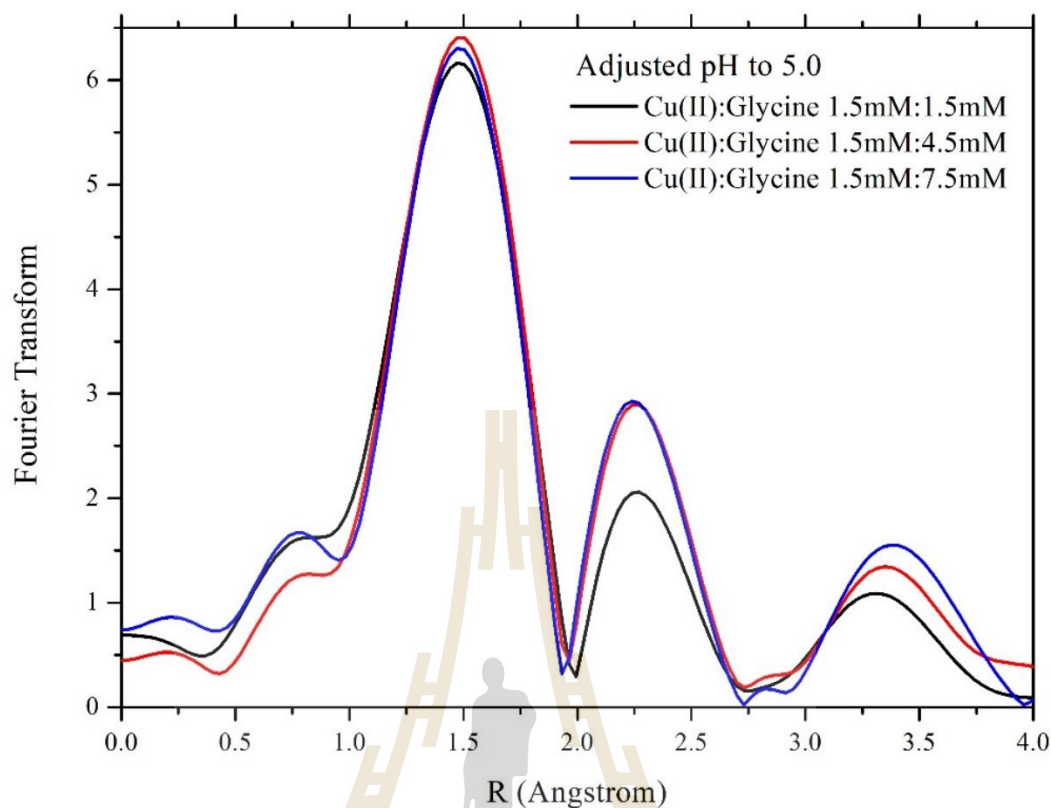
adjusted pH value to 5.0.

Figure 4.13 Fourier transforms of Cu(II):Glycine in 1.5mM:1.5mM to 1.5mM:7.5mM

with adjusted the pH value to 5.0.

As the Fourier transforms of Cu(II):Glycine at molar ratio 1.5mM: 7.5mM with adjusted pH value to 5.0, the amplitude at second shell is obviously increased and There is a complex solution: $CuGly_2$ species (Darj *et al*., 1996). To support the idea of Cu(II):Glycine at molar ratio 1.5mM:7.5mM with adjusted pH value to 5.0 is $CuGly_2$ species by using model fitting. This analysis was useful to a got accurate results. Moreover, the study second and third shells of the aqueous solution of CuCl2 in concentration 1.5mM and Cu(II) mixed with glycine in concentration 1.5mM:7.5mM by adjusting the pH value to 5.0. The more details for fitting are shown in the part of Appendix B.
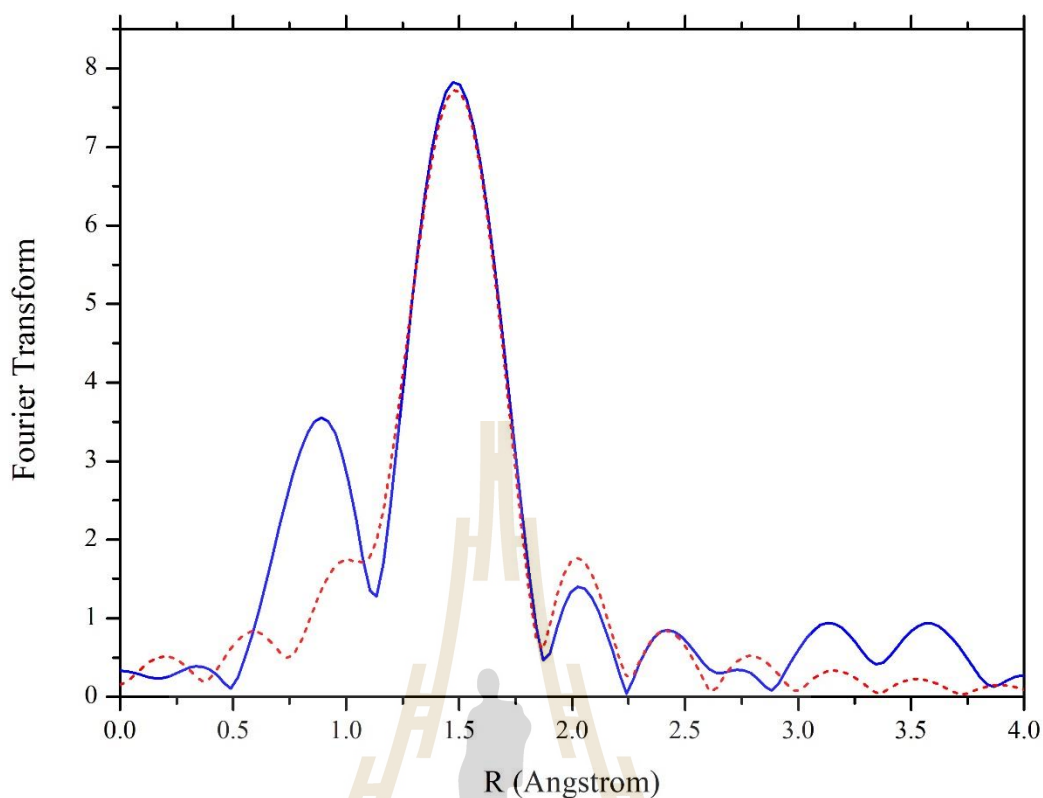
Figure 4.14 Fourier transforms of Cu(II) standard at 1.5 mM, blue line is experiment
and red dot line is fitting.

Figure 4.14 showed Fourier transform of Cu(II) standard at 1.5 mM compared
with Cu(II):Glycine 1.5mM:7.5mM with adjusted the pH value to 5.0. FTs of Cu(II)
standard has been calculated in the interval k = 3-11.5 Å^{-1} as shown in Figure 4.14(a).
The first peak in the shift-corrected FT at 1.94 ± 0.014 Å is indicated of the Cu-O signal.
The second peak in FT at 2.13 ± 0.062 Å is indicated of the Cu-O$_{ax}$ signal and the third
peak in FT at 2.26 ± 0.192 Å is accounted for the Cu-H signal. The detail each parameter
showed in Table 4.3.

Table 4.3 The parameters of Cu(II) standard at 1.5 mM.

Structure feature	S_0^{2*}	CN	σ^2 (Å²)	R (Å)
Cu-O	0.915	3.85 ± 0.04	0.003	1.94
Cu-O$_{ax}$	0.915	1.87 ± 0.04	0.007	2.13
Cu-H	0.915	3.85 ± 0.04	0.012	2.26

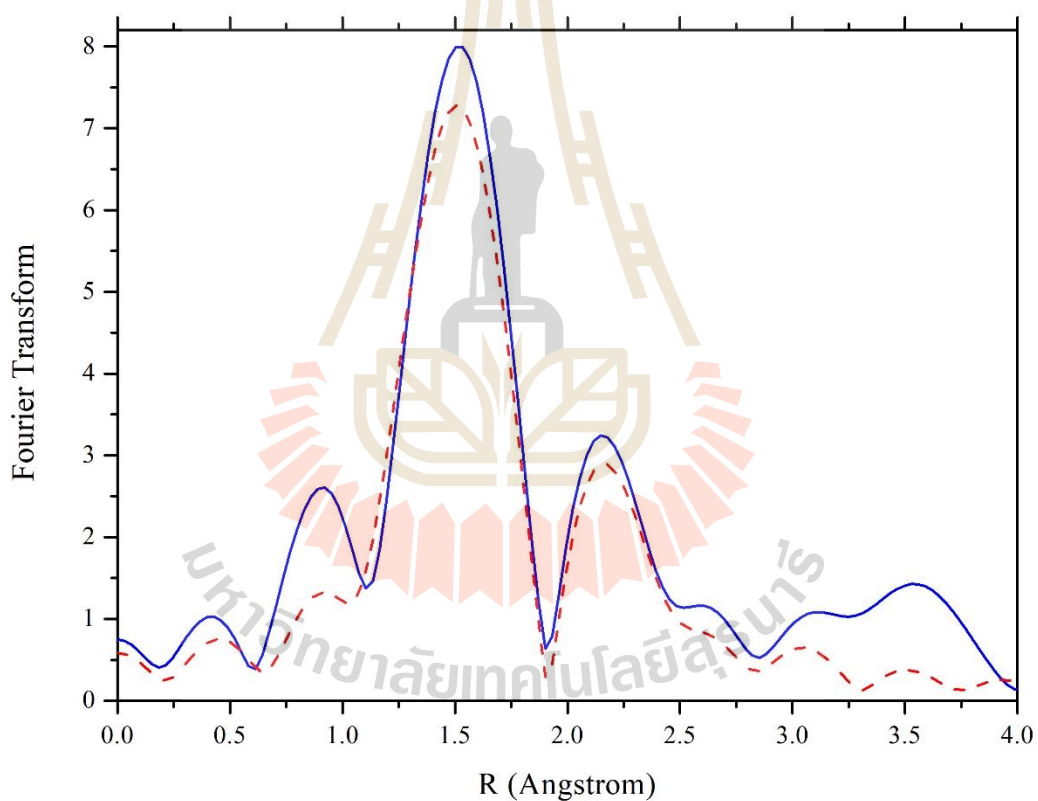* the S_0^2 value is comes from copper foil fitting.

Figure 4.15 Fourier Transform of Cu(II):Glycine 1.5mM:7.5mM with adjusting the pH

value to 5.0: blue line is experiment and red dash line is fitting.

For the EXAFS spectrum of Cu(II):Glycine 1.5mM:7.5mM with adjusting the

pH has been performed by in the range k = 3-10.2 Å^{-1} as shown the Figure 4.15. The

first peak in the shift-corrected FT at 1.95 ± 0.014 Å is indicated of the Cu-Glycine signal that comes from oxygen in the glycine molecule. The second peak in FT at 2.64 ± 0.056 Å is indicated of the $Cu-O_{ax}$ signal and the third peak in FT at 2.82 ± 0.061 Å is accounted for the Cu-C signal.

Table 4.4 The parameters of Cu(II):Glycine 1.5mM:7.5mM with adjusted the pH value to 5.0.

Structure feature	S_0^2	CN	σ^2 (Å^2)	R (Å)
Cu-O	0.915	3.39 ± 0.22	0.004	1.95
$Cu-O_{ax}$	0.915	1.68 ± 0.22	0.009	2.64
Cu-C	0.915	3.39 ± 0.22	0.010	2.82

* the S_0^2 value is comes from copper foil fitting.

CHAPTER V

CONCLUSION

In this research, a structural changes of Copper (II) chloride aqueous solution mixed with glycine aqueous solution was investigated by X-ray absorption spectroscopy (XAS) technique. The X-ray absorption near edge structure (XANES) and the extended X-ray absorption fine structure (EXAFS) measurements were performed at beamline 1.1W: multiple X-ray techniques of synchrotron light research institute (SLRI), Thailand for understanding the local structure of Cu(II):Glycine solution and coordination shell of copper(II) metal.

The Copper *K*-edge spectra of Copper (II) chloride aqueous solution mixed with glycine aqueous solution were obtained by varying molar ratio of Cu(II):Glycine solution. Investigation on XANES spectra of standard reference of copper and $CuCl_2$ solution indicated Cu(II):Glycine solution. Moreover, characterization of the absorption spectra proposed the spectral fingerprint for Cu(II):Glycine complex as formerly studied (Chaboy *et al.*, 2005). In term of EXAFS analysis, the data provided the structural information at different Cu(II):Glycine molar ratios. In particular, the pH values measured are important, thus causing major and minor copper species. Changes in pH value affected the coordination shell of the metallic center as observed from EXAFS results. After that the different molar ratio of Cu(II):Glycine were prepared and driven to the single major species of copper complex solution by controlling pH adjustment of 5.0. The results support that the species of copper complex with glycine

was pH dependent and affected the structural features investigated by both XANES and EXAFS. The benefit of this study is to understand the condition to form copper-glycine species.

It was found that $CuCl_2$ powder and glycine powder have a different solubility in water. Therefore, the initial concentration is 2.5 M in a 25 mL of water that is the most suitable. It is note that, to reduce the problems caused by saturation of the solution, the highest concentration used for measurement is 0.5 M for both of Cu(II) chloride and glycine aqueous solutions. It is interesting to be caution with the problem caused by the transition form of the aqueous solution. To minimize this problem the solutions should not be prepared for more than 1 hour before the measurements.
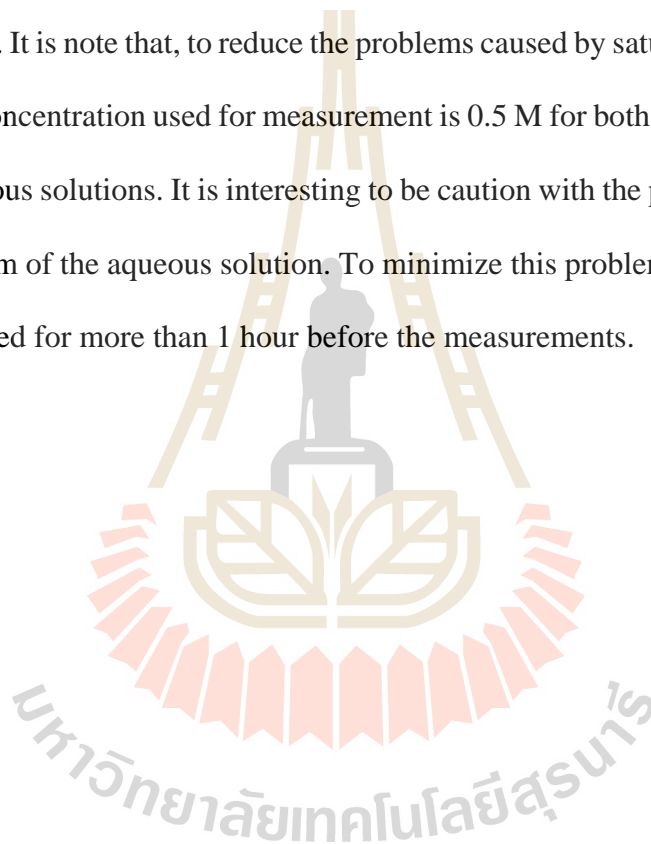
REFERENCES
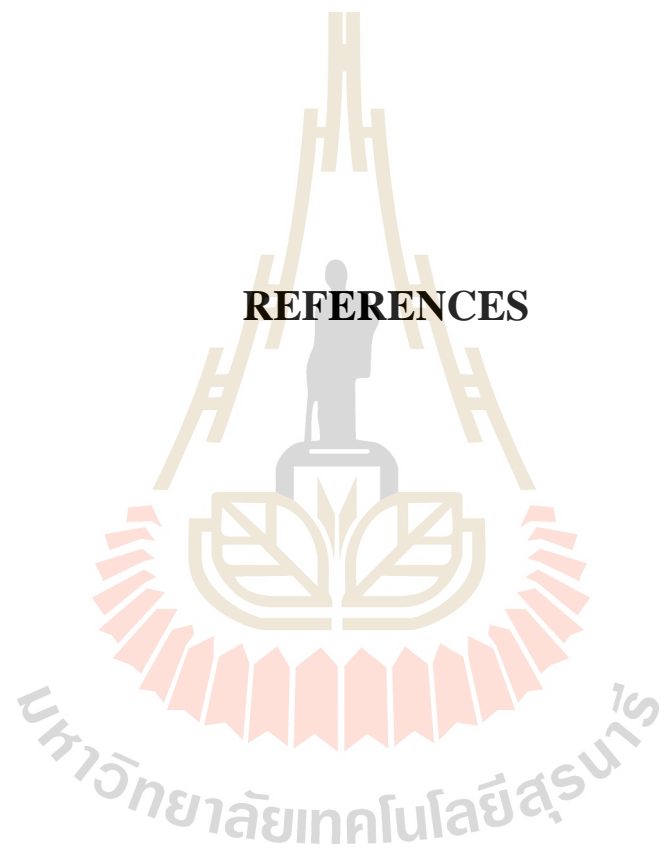
REFERENCES

Atipong, B. (2014). Local structure and dielectric properties of barium titanate-based relaxor ferroelectrics. Suranaree University of Technology, Nakhon Ratchasima.

Borsook, H., and Thimann, K. V. (1932). The cupric complexes of glycine and of alanine. **J. Biol. Chem.** 98:671

Carrera, F., Marcos, E. S., Merkling, P. J., Chaboy, J., and Muñoz-Páez, A. (2004). Nature of metal binding sites in Cu(II) complexes with histidine and related N-coordinating ligands, as studied by EXAFS. **J. Inorg. Chem.** 43: 6674.

Chaboy, J., Muñoz-Páez, A., Carrera, F., Merkling, P., and Marcos, E. S. (2005). Ab initio x-ray absorption study of copper K-edge XANES spectra in Cu(II) compounds **J. Phys. Rev. B**. 71: 134208.

D'Angelo, P., Bottari, E., Festa, M. R., Nolting, H. F., and Pavel, N. V. (1997). Structural investigation of copper(II) chloride solutions using x-ray absorption spectroscopy **J. Chem. Phys.** 107: 2807.

D'Angelo, P., Bottari, E., Festa, M. R., Nolting, H.-F., and Pavel, N .V. (1998). X-ray absorption study of copper(II)-glycinate complexes in aqueous solution. **J. Phys. Chem. B**. 102: 3114.

Darj, M. M., and Malinowski, E. R. (1996). Complexation between copper(II) and glycine in aqueous acid solutions by window factor analysis of visible spectra. **J. Anal. Chem.** 68: 1593.

European Food Safety Authority (EFSA), (2015). Scientific opinion on Dietary Reference values for copper. **J. EFSA**. 13(10): 4253.

Hasnain, S. S., Murphy, L. M., Strange, R. W., Grossmann, J. G., Clarke, A. R., and Jackson, G. S. (2001). XAFS study of the high-affinity copper-binding site of human PrP[91-231] and its low-resolution structure in solution **J. Mol. Biol.** 311: 46.

Konishi, H. (2007). Selective separation and recovery of copper from iron and mixed waste by ammonia solution. **ISIJ International**. 36: 73-71.

Lee, P. A., Citrin, P. H., Eisenberger, P., and Kincaid, B. M. (1981). Extended x-ray absorption fine structure-it strength and limitations as a structural tool. **Rev. Mod. Phys.** 53: 4.

Moira, E. M. (2013). Magnesium and Copper(II) Chloride: A Curious Redox Reaction. Indiana University of Pennsylvania.

Newville, M. (2001). IFEFFIT: interactive XAFS analysis and FEFF fitting. **J. Syn. Rad.** 8: 322.

Wantana, K. (2012). X-ray Absorption Spectroscopy Technique at Siam Photon. Nakhon Ratchasima, **Thailand:Synchrotron Light Research Institute**.

Schnohr, C. S., and Ridgway, M. C. (2015). Introduction to X-ray Absorption Spectroscopy. **Spring Series in Optical Science.** 190.
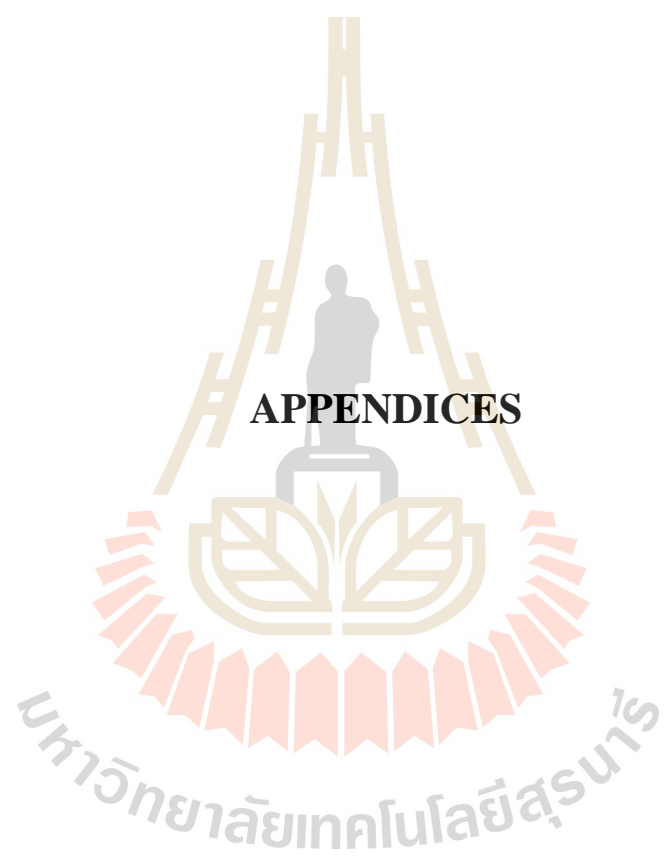
APPENDICES

APPENDIX A

NORMALIZATION OF SPECTRA

Athena program used for analysis XANES spectra from XAS spectra. For Athena program can be downloaded by link

Procedure for Athena program

1. Open the program that has the icon , when the program opened the window as shown in the figure A.1., the program consisted 5 sub windows

(I) The main window shows the currently of name and parameters data.

(II) The window shows order of data that import into the Athena program.

(III) The window shows the details, suggestion, and error of data.

(IV) The window shows parameters that plot in spectrum; such as pre-edge, post-edge, Normalization, Derivation, and second derivative.
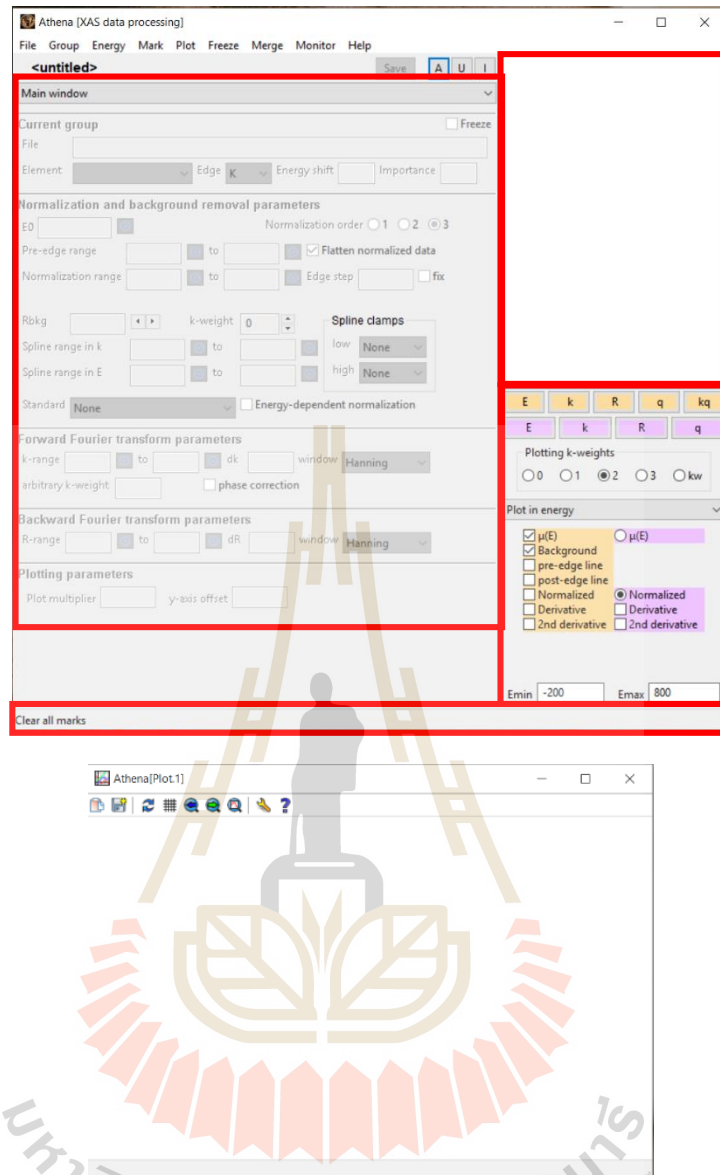
(V) The window shows the results of spectrum.

Figure A.1 The main window of the Athena program.

2. Select file that wants to import to analyzation. The first of all data, you should
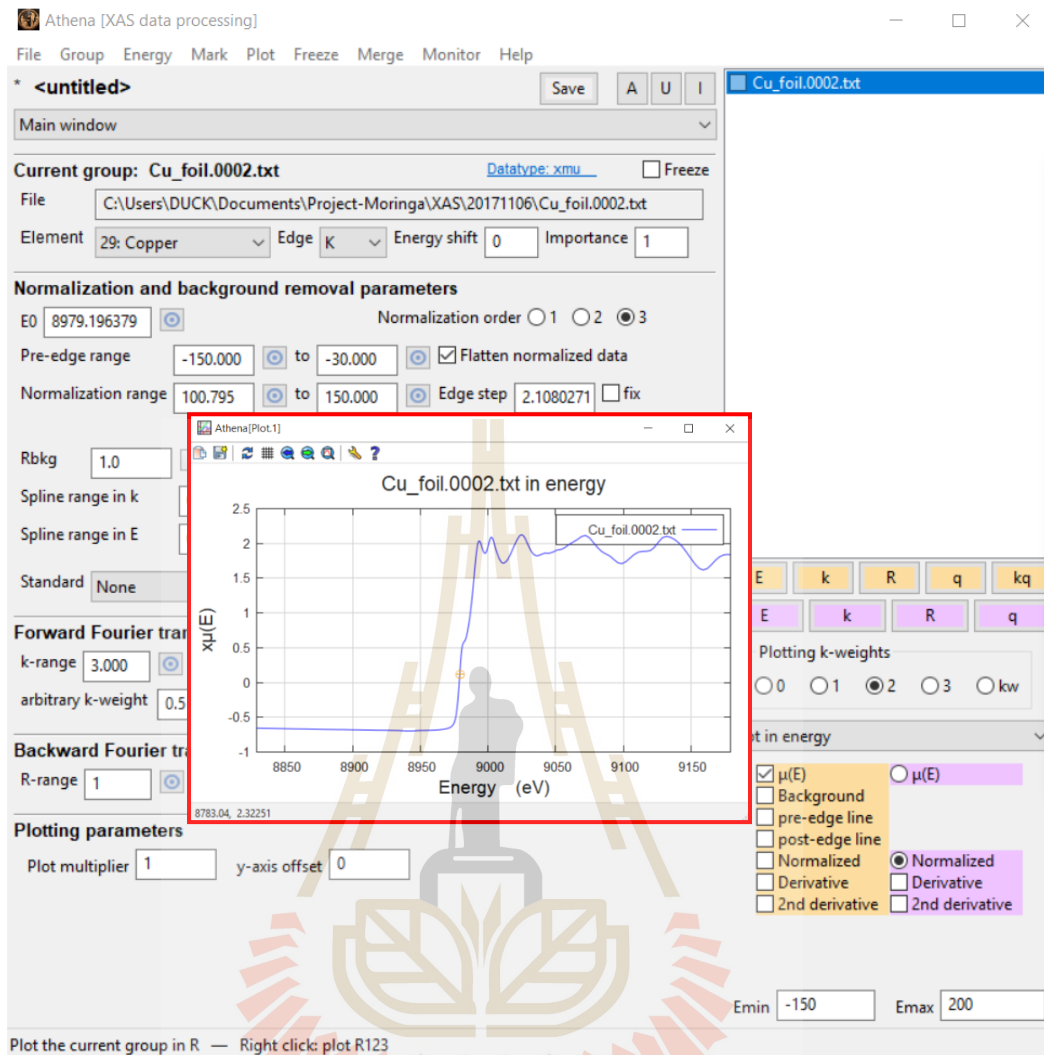
import the copper foil, that shown in the figure A.2.

Figure A.2 Importing of data

3. When already to choose the copper foil, the window shown as a figure A.3.

Figure A.3 The pop-up window when import copper foil.

4. At BL 1.1w, they have measured foil at the same time as a sample. We will calibrate the energy of the copper foil for used the energy shift to the calibration of a sample. When the pop-up window show as below, choose "select a point" and double click at the middle of derivative peak and go to click "Calibrate", the energy of copper will go to 8979 eV.
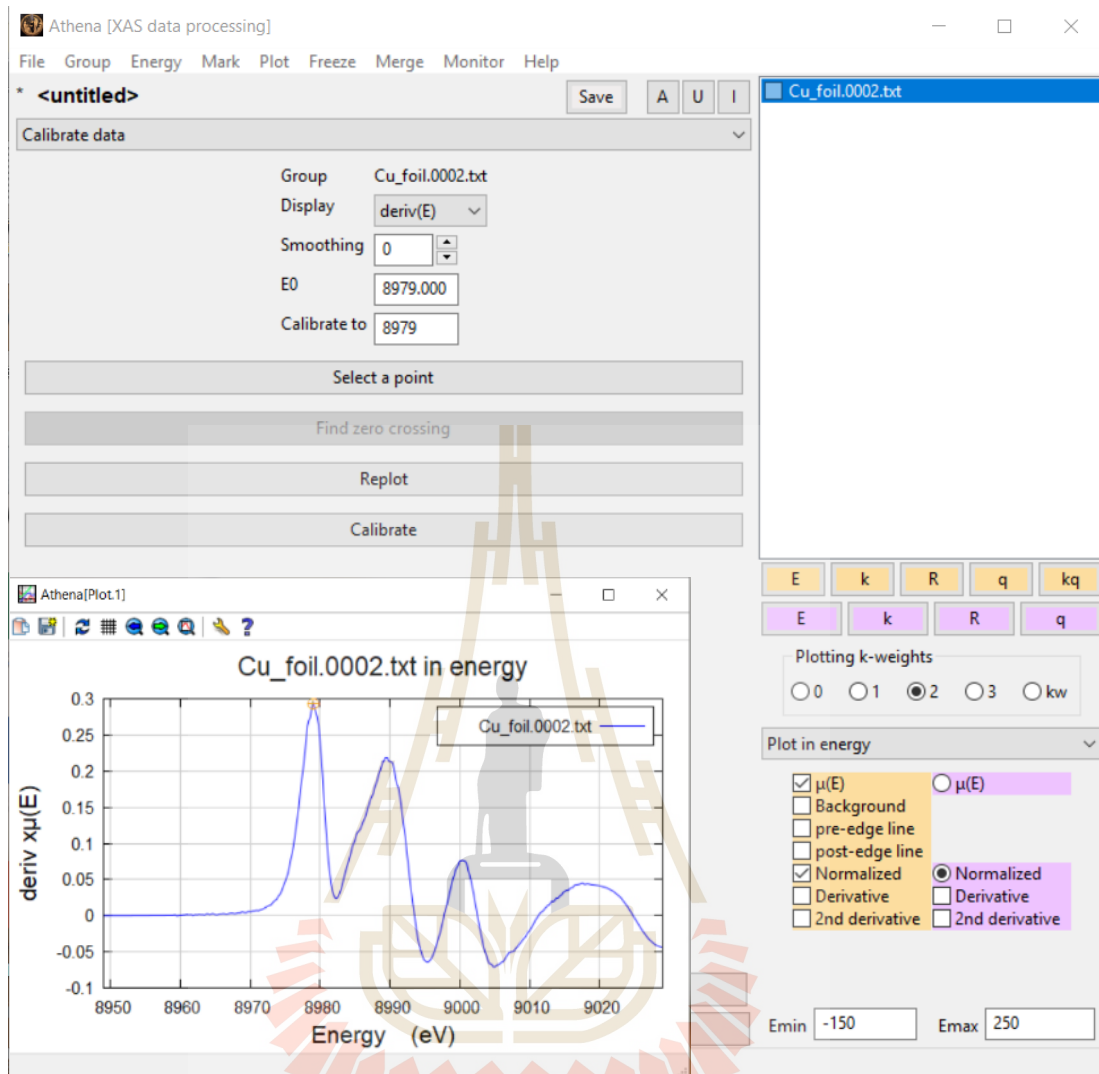
Figure A.4 The calibration of copper foil.

5. Go to the normalization of copper foil, choose "pre-edge" and "post-edge" for

normalization energy $\mu(E)$. The pre-edge and post-edge line as shown in figure A.5.
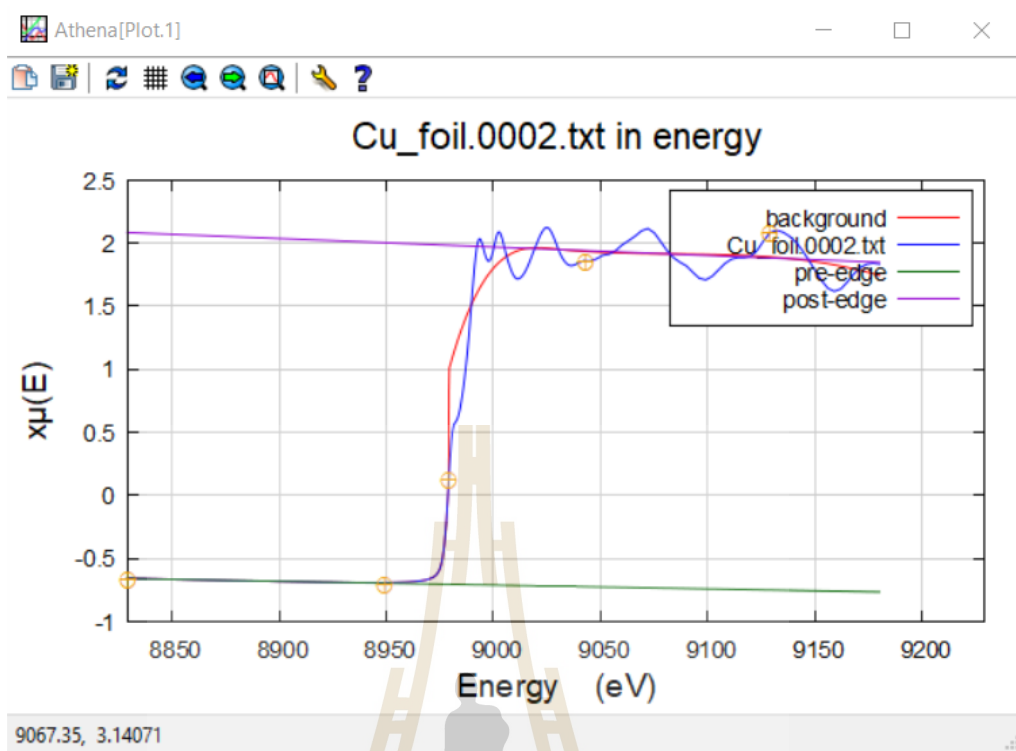
Figure A.5 The normalization of data, background (red line), the copper foil data (blue

line), pre-edge (green line), and post-edge (purple line).

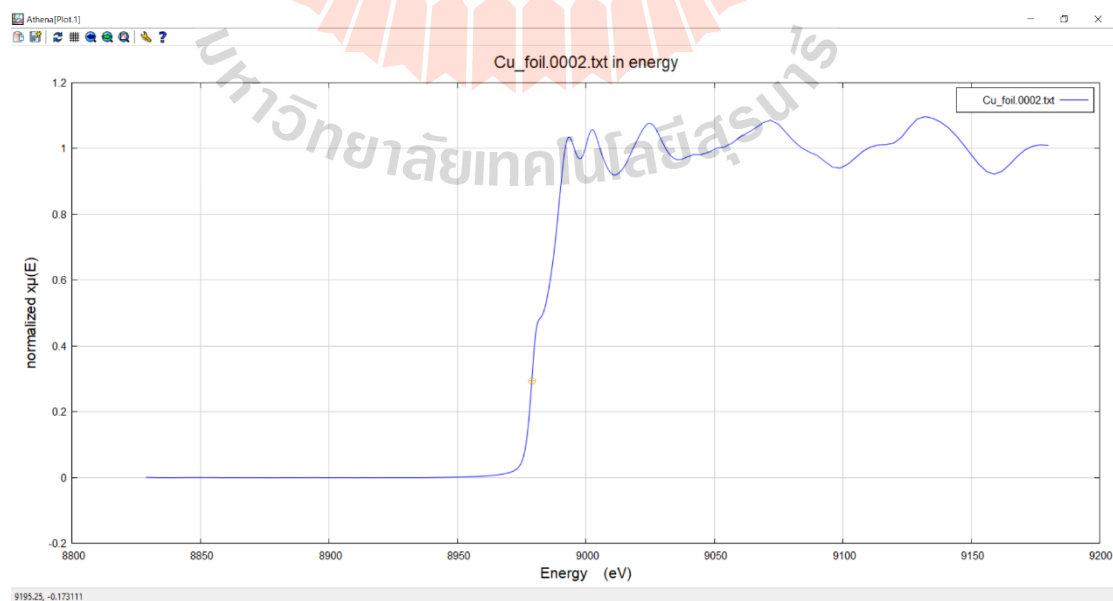6. Finally, the copper foil data that normalized energy as show in figure A.6.

Figure A.6 The copper foil spectrum after normalization.

APPENDIX B

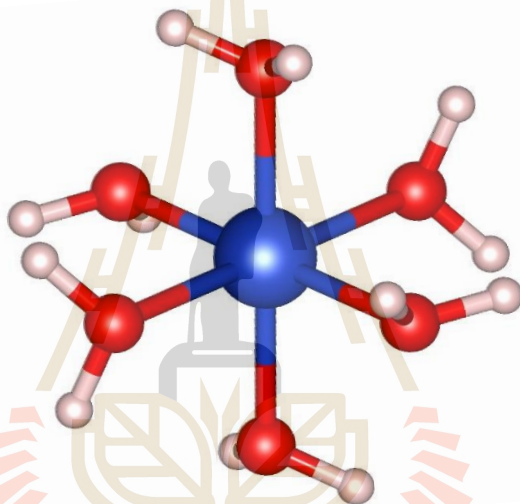# EXAFS FITTING

1. Cu(II) standard for concentration at 1.5mM

Figure B.1 Octahedral structure of Cu·6H$_2$O that used for fitting standard solutions:

blue is Copper, red is oxygen, and white is hydrogen.
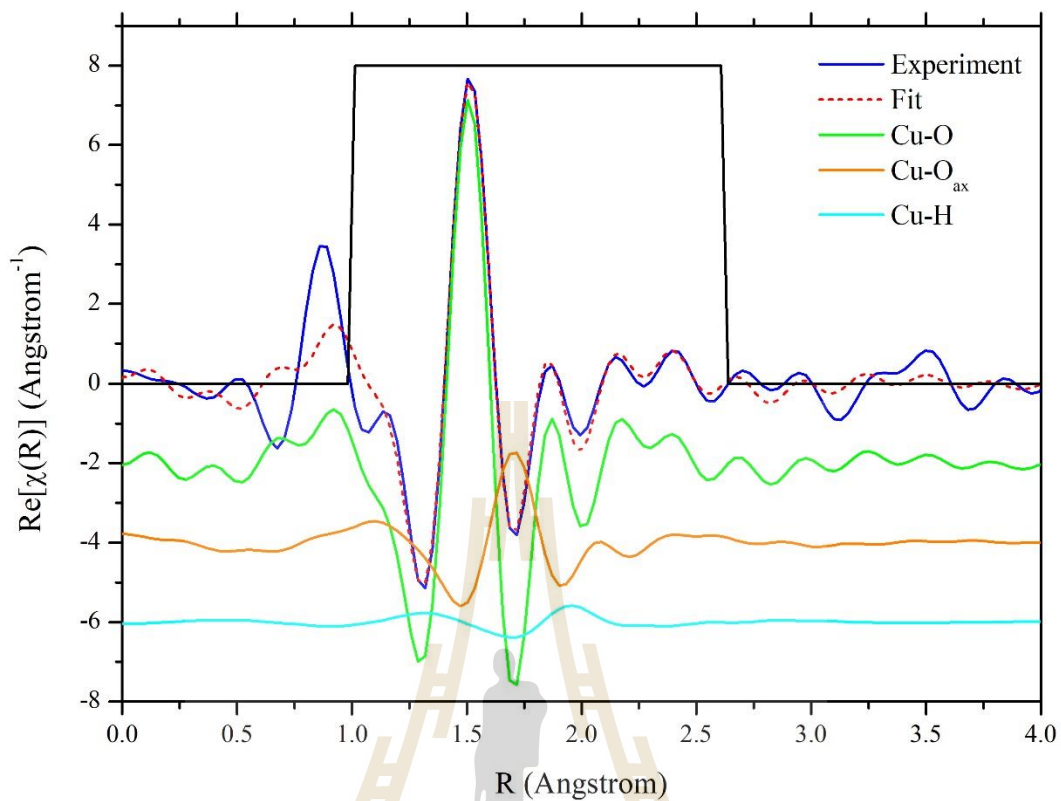
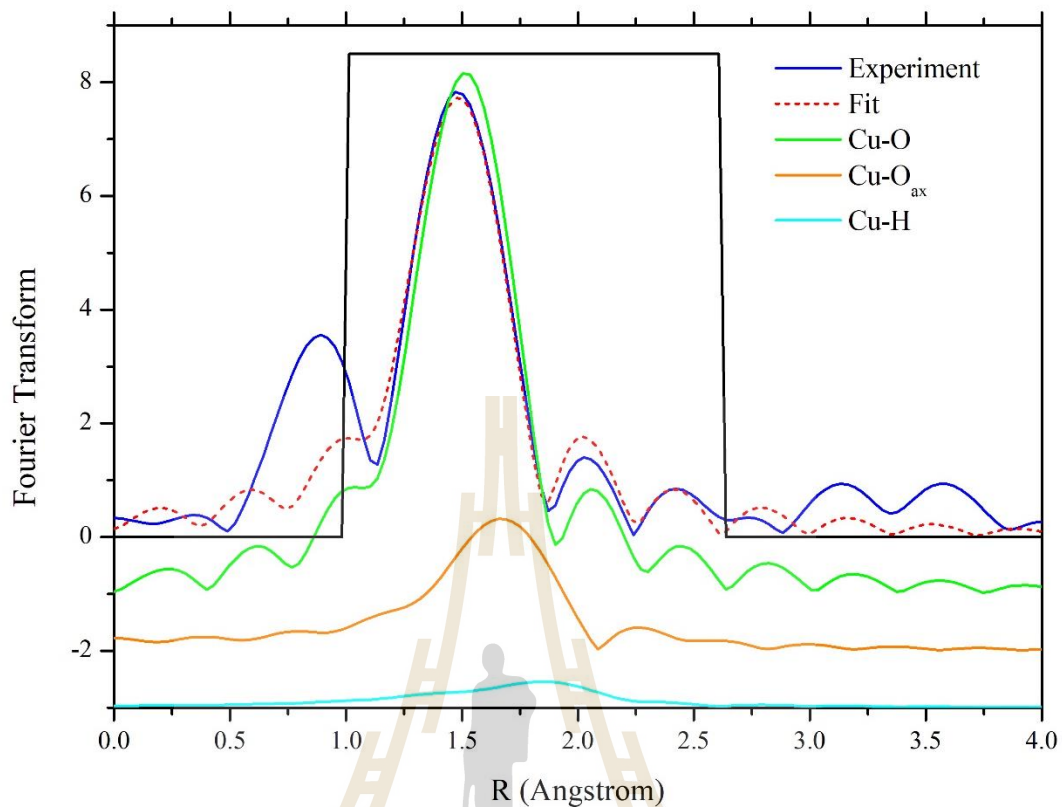**Figure B.2** Fourier Transform in the real-part as a function of radial distance for standard solution of 1.5mM CuCl$_2$

Figure B.3 The radial distance standard solution of 1.5mM CuCl₂.

2. Cu(II):Glycine for concentration 1.5mM:7.5mM with adjusted the pH value to 5.0.

The modeling for Cu:Glycine solution in concentration 1.5mM:7.5mM with adjusted pH to 5.0 showed in Figure B.4.
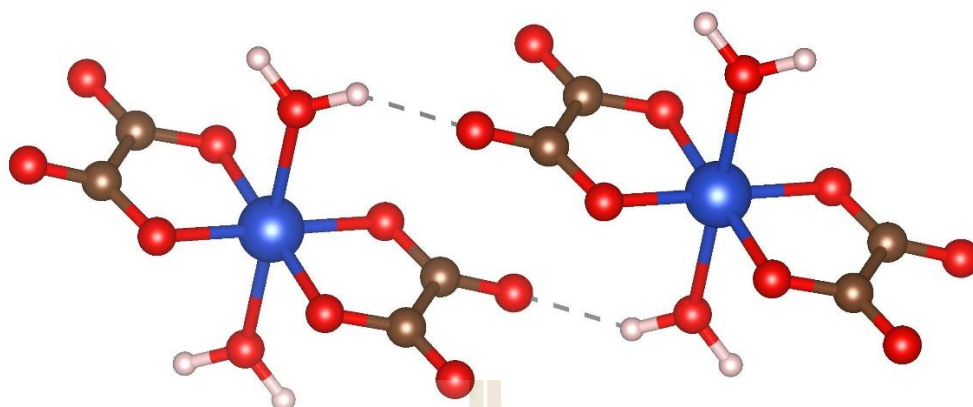
Figure B.4 The structure of $CuH_{11}C_4(NO_5)_2$ that used for fitting mixture solutions: blue

is Copper, red is oxygen, brown is carbon, and white is hydrogen.

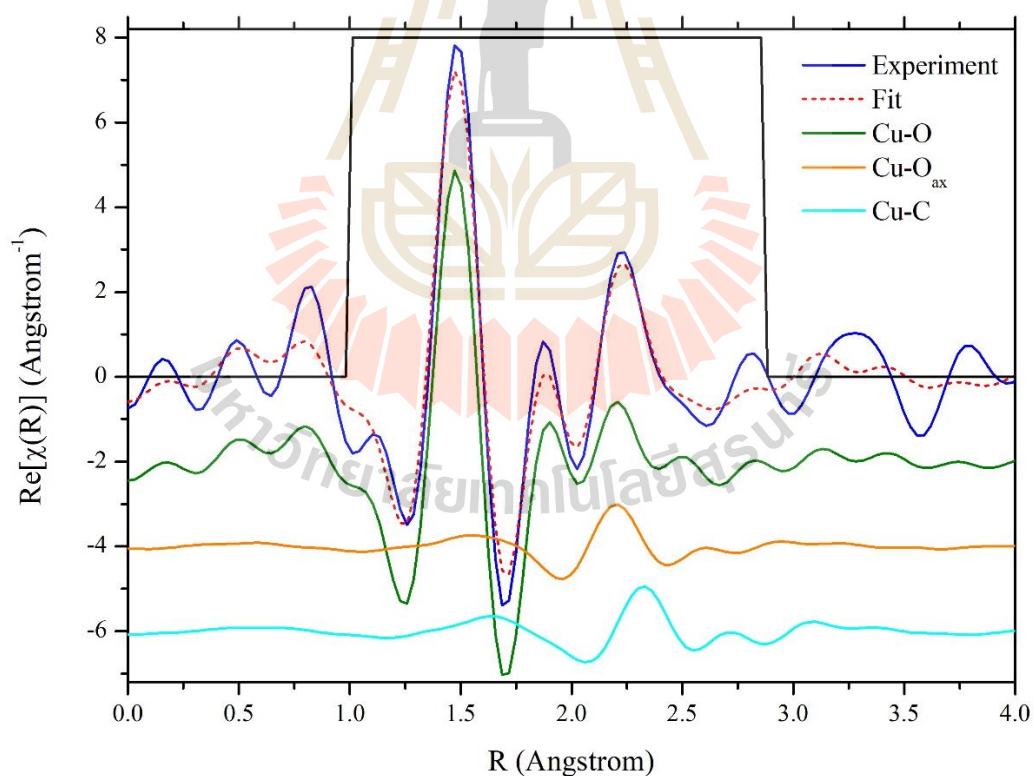**Figure B.5** Fourier Transform in the real-part as a function of radial distance for

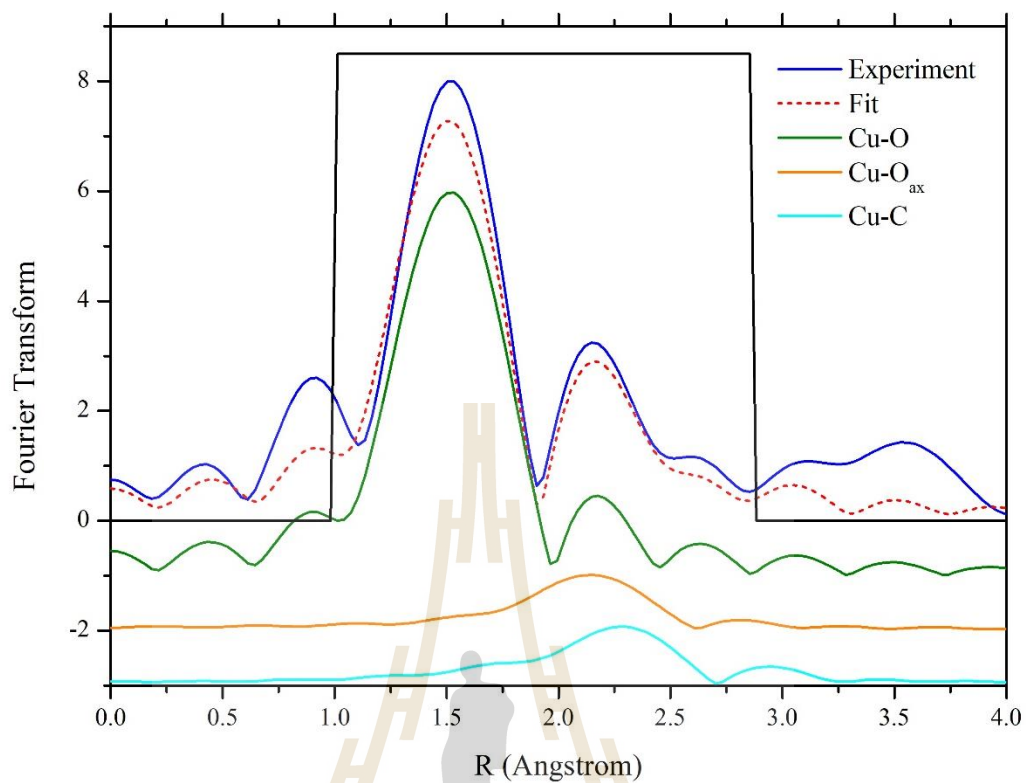standard solution of Cu(II):glycine 1.5mM:7.5mM with adjusted pH to 5.0.

Figure B.6 The radial distance of Cu(II):glycine 1.5mM:7.5mM with adjusted pH to

5.0.

CURRICURUM VITAE

Name   Kanchanasuda Klaiphet

Date of Birth   25 March 1994

Place of Birth   Phrae, Thailand

Education

- 2012 – 2015   Bachelor of Science in Physics, Department of Physics, Facalty of Science, Naresuan University, Phitsanulok, Thailand

- 2016 – present   Master of Science in Physics, School of Physics, Institute of Science, Suranaree University of Technology, Nakhon Ratchasima, Thailand

Publication "Structural study of Cu(II):Glycine solution by X-ray absorption spectroscopy", K. Klaiphet, T. Saisopa, W. Pokapanich, S. Tangsukworakhun, C. Songsiriritthigul, C. Saiyasombat, D. Céolin and P. Songsiriritthigul, Journal of Physics: Conference Series 1144 (2018): 012063.